Structures 68 (2024) 107090

Contents lists available at ScienceDirect

Structures

journal homepage: www.elsevier.com/locate/structures

Numerical investigations of seismic-resilient techniques for legged fluid storage tanks utilising magnetorheological dampers

Seyed Ehsan Aghakouchaki Hosseini *, Sherif Beskhyroun

Department of Built Environment Engineering, Faculty of Design and Creative Technologies, School of Future Environments, Auckland University of Technology (AUT), 1010 Auckland, New Zealand

ARTICLE INFO

Keywords:
Fluid storage tanks
Seismic-resilient structures
Semi-active control
MR dampers
Hunger game search

ABSTRACT

Different energy-dissipating devices have been proposed in the literature to attenuate the destructive effects of base excitations over fluid storage tanks. These structures have numerous applications in strategic industries and their failure can result in environmental hazards and huge economic losses. Proposed techniques in the literature for seismic energy dissipation of fluid-contained tanks are mostly centred on passive and active control mechanisms. Semi-active control devices using materials with adjustable properties offer advantages of both active and passive systems while removing their drawbacks. In this paper, the performance of a Magnetorheological (MR) damper on the seismic response reduction of fluid storage tanks through the application of three different control strategies including H2/LQG, PID, FOPID, and two passive techniques, i.e. Passive On, and Passive Off has been investigated. Parameters of the semi-active controllers are optimally designed for each aspect ratio and the applied ground motion using the Hunger Game Search (HGS) technique and finally, the semi-active Clipping algorithm commands the voltage to the damper. The fluid-tank-MR damper system has been examined under three Far-Fault and three Near-Fault ground motions. Numerical simulations have demonstrated that depending on the aspect ratio, applied ground motion, and the control strategy, the MR damper can mitigate the peak relative displacements and absolute accelerations of the two major modes of the system, i.e the rigid and impulsive modes, up to 72% and 67%, respectively. This proves the efficacy of these dampers in reducing the maximum base shear and overturning moment, hence mitigating the damage risks in these structures.

1. Introduction

Fluid storage tanks are widely used in a variety of applications and industries with strategic importance and play a critical role in the stability and functionality of the corresponding industries. They are used for the storage of various liquids like water, wine, dairy products, oil, etc. in wineries, refineries, nuclear power plants, and so on. Ground-supported fluid storage tanks which, depending on their applications, may contain various types of fluids, are usually applied for storage, distribution, or processing of the contained liquid. Aspect ratio defined as liquid height to the radius or length of the tank's cross section for circular and rectangular tanks, respectively, plays an important role in their dynamic behaviour under vibrations. These structures are considered as acceleration-sensitive elements in FEMA 274 [1]. Such tanks are susceptible to damage in earthquake-prone regions of the world [2–6]. Two of the most common types of damage to fluid storage tanks during earthquakes are elephant foot and diamond-shaped buckling. However, other types of damage including damage to the base connections such as anchor bolt buckling, elongation and/or pull-out, leg buckling, damage to the roof due to liquid sloshing, rupture of the shell, etc. can occur depending on the type of support, aspect ratio and size of the tank, and their application, among others. Any damage to these tanks may cause adverse environmental effects, jeopardise their integrity, risk human life, and result in disastrous consequences.

Analysing structural behaviour and dynamic modelling of these structural systems has been the focus of attention by different researchers for decades [7–9]. Different types of damage caused in previous devastating seismic events have been examined and various energy-dissipating devices have been proposed by researchers in the literature [10]. A comprehensive review of different dynamic modelling methodologies, seismic protection devices proposed, and various types of damages observed in previous seismic events have been conducted by authors [11]. Among various modelling techniques proposed so far for these structures, the lumped parameter model which is an equivalent mechanical model representing the complex fluid–structure interaction has been widely used for analysing the structural responses

* Corresponding author.
E-mail addresses: ehsan.hosseini@autuni.ac.nz (S.E.A. Hosseini), sherif.beskhyroun@aut.ac.nz (S. Beskhyroun).

https://doi.org/10.1016/j.istruc.2024.107090
Received 27 March 2024; Received in revised form 24 July 2024; Accepted 13 August 2024
Available online 19 August 2024

of these structures [7]. This technique has formed the basis of the structural design of tanks in different seismic codes including Eurocode 8 Part 4 [12] and NZSEE [13]. Validation of this technique has been studied by several researchers [14]. While this methodology provides dynamic characteristics of the vibration of the highly complex fluid–structure interaction in a fluid tank with acceptable accuracy they offer efficient and low computational effort compared to more sophisticated Finite Element (FE) based techniques [11].

Vibration control systems and techniques have been targeted for decades to enhance the safety, reliability, and resiliency of engineering structures against undesirable vibrations, especially those caused by severe earthquakes. Passive control mechanisms offer reliability whereas they are not adaptable or versatile. On the other hand, active control systems, while removing drawbacks of passive systems, rely on considerable external power for their operation which could be a source of substantial concern during a disaster. Moreover, reliability and robustness are always matters of concern for active systems. Semi-active systems aim to combine the advantages of both passive and active systems while eliminating their weak points. Application of a semi-active variable stiffness damper in combination with two passive systems including Elastomeric Rubber Bearing (ERB) and Lead Rubber Bearing (LRB) also called N-Z system [15,16] for seismic protection of a horizontally curved bridge has been examined in [17]. Passive control devices for energy-dissipation and seismic protection of fluid storage tanks and industrial plants have been developed and applied to these structures in different forms now for decades [18]. Base isolators and their variants [19–21], Horizontal and vertical baffles [22,23], are amongst the most developed passive systems for fluid tanks. Active baffles [24] and piezoelectric patches [25] can be named as instances of active devices proposed in this field. Semi-active control devices for vibration control and seismic protection of fluid-contained tanks and vessels have not been explored to the same extent as passive and active systems. Examples of such devices include variable dampers for making smart base isolation [26], the semi-active mechanism proposed by Kobayashi and Koyama [27] based on the air spring effect of a gas chamber, and the application of Magnetorheological (MR) dampers by Shrimali and Kasar [28]. The study by Shrimali and Kasar [28] considered the utilisation of MR dampers between two adjacent tanks for the aim of seismic response reduction of connected liquid storage tanks. Authors believe that the effects of employing these dampers over the vibrational responses of these strategic structures under seismic base excitations have not been comprehensively examined.

MR dampers are based on smart MR fluid with adaptable properties. Physical properties such as the viscosity of such a fluid can be changed in a few milliseconds [29,30] upon the application of a magnetic field. Thus, the interactive force produced by the damper can be rapidly controlled and adapted according to the force required at each time step to counteract the applied external force on the system. These dampers are fail-safe as in case of any malfunction in the control system they are turned into passive devices (Passive Off mode) and still can continue damping the vibrations. Special features of these dampers such as a wide operational temperature range, and high achievable yield stresses, to name but a few, have enabled this possibility to apply them in a variety of interior and exterior applications for seismic and vibration mitigation of civil structures and infrastructures as well as other industrial applications [31]. Performance of an MR damper as a variable damper for seismic protection of highway bridges has been discussed in [32]. Chen et al. investigated the performance of MR dampers in smart base isolation systems using real-time hybrid tests [33]. Prakash and Jangid studied the results of coupling an MR damper with a nonlinear isolation system called Unbonded Fibre-Reinforced Elastomeric Isolator (UFREI) over the structural response mitigation of a full-scale three-story benchmark building [34].

Legged steel fluid storage tanks are widely used in different industries including the wineries, dairy products industries, petrochemicals, etc. for storage of oil, water, and other chemicals [35–37]. A research effort on the effects of employing MR dampers on the seismic response mitigation of legged fluid storage tanks was initiated by the authors [38]. In this paper, the application of MR dampers for vibration attenuation of a legged ground-supported fluid storage tank against seismic actions is investigated numerically in detail. The connections of the legs to the base are considered fixed and the tank shell is regarded as flexible. Based on these assumptions and using the simplified mechanical model proposed in the literature [7,8,39–41] and seismic design codes [13] for the dynamic behaviour of fluid tanks, the equation of motion for the coupled fluid-tank-damper system is formulated. To model the nonlinear hysteretic behaviour of MR dampers, the modified Bouc–Wen model [42–45] is employed. To perform a semi-active vibration control technique to the considered fluid-tank system, three control strategies including the H2/Linear Quadratic Gaussian (H2/LQG) [44,46–49], the Proportional–Integral–Derivative (PID) [50,51], and the Fractional order PID (FOPID) [45,52,53] which have demonstrated desirable performances in variety of control applications have been utilised. Each controller has some parameters which need to be designed appropriately to achieve a desirable control action and satisfy the control objective. In this research an optimisation technique termed Hunger Game Search (HGS) [54] which has proved promising features in the literature has been employed to design the parameters of each controller. Due to the nature of the semi-active control mechanism the calculated active control force cannot be commanded, a secondary control technique is required to adjust the required voltages to the MR damper. To this aim, the clipping control approach [29,44,55,56] has been regarded. Numerical simulations of a legged cylindrical stainless steel fluid storage tank equipped with an MR damper under the El Centro 1940, the Hachinohe 1968, and the Manjil 1990 as Far-Fult and the Kobe 1995, the Northridge 1994, and the Tabas 1978 as Near-Fault ground motions have been presented. The efficiency of the damper in reducing the tank's seismic responses using the employed semi-active control techniques for different aspect ratios and under the applied base excitations with different frequency contents has been studied and compared.

2. Dynamic modelling of the coupled system

The schematic of a flexible legged circular cylindrical fluid storage tank equipped with an MR damper connected rigidly in a horizontal direction between the tank base and the ground through one of its legs, as shown in Fig. 1 is considered. This tank has been regarded as made of stainless steel material for both the shell and the legs. Legs are made of tubular cross-sections. Dimensions and profiles of the tank and legs with their cross sections can be found in this figure. The connections of the legs to the base have been considered fixed. This tank is filled with water up to a height of H_l. The equivalent mechanical representation of the physical MR damper-tank-fluid system is shown in Fig. 2.

Assuming the tank body will not enter the material nonlinearity region while undergoing vibrations, the dynamic equation of motion for the coupled fluid-tank-MR damper system shown in Fig. 2 is written according to Eq. (1),

$$M\ddot{U}(t) + C\dot{U}(t) + KU(t) = \xi F_{MR} - M\lambda\ddot{u}_g(t) \tag{1}$$

where, M, C, and K are the mass, damping, and stiffness matrices, F_{MR} and $\ddot{u}_g$ are the MR damper force and ground acceleration, ξ and λ are position vectors, and the vectors $\ddot{U}$, $\dot{U}$ and U are acceleration, velocity, and displacement vectors of lumped masses shown in Fig. 2, respectively. These matrices and vectors are defined as follows,

$$M = \begin{bmatrix} m_r & 0 & 0 \\ 0 & m_i & 0 \\ 0 & 0 & m_c \end{bmatrix}, C = \begin{bmatrix} c_r + c_i + c_c & -c_i & -c_c \\ -c_i & c_i & 0 \\ -c_c & 0 & c_c \end{bmatrix}, K = \begin{bmatrix} k_r + k_i + k_c & -k_i & -k_c \\ -k_i & k_i & 0 \\ -k_c & 0 & k_c \end{bmatrix} \tag{2}$$

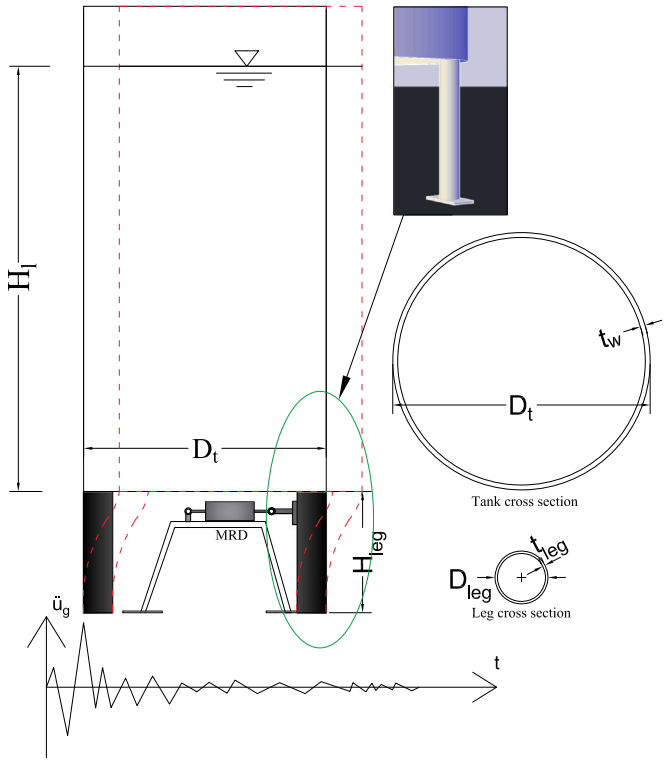

Fig. 1. Schematic of MRD-fluid-tank system.

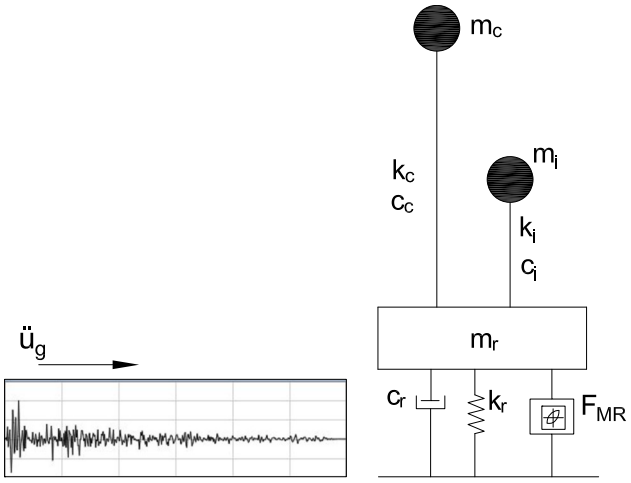

Fig. 2. Mechanical representation of the MRD-fluid-tank system.

$$\ddot{U} = \begin{bmatrix} \ddot{u_r} \\ \ddot{u_i} \\ \ddot{u_c} \end{bmatrix}, \dot{U} = \begin{bmatrix} \dot{u_r} \\ \dot{u_i} \\ \dot{u_c} \end{bmatrix}, U = \begin{bmatrix} u_r \\ u_i \\ u_c \end{bmatrix}, \xi = \begin{bmatrix} -1 \\ 0 \\ 0 \end{bmatrix}, \lambda = [1]_{3\times1} \tag{3}$$

In this representation, the tank shell has been considered flexible, and only the first impulsive and the first convective modes are considered. Mass, damping, and stiffness of these modes are shown as m_i, m_c, c_i, c_c, k_i, k_c, while m_r is the fluid mass that moves rigidly with the tank shell. The c_r and k_r represent the damping and stiffness associated with the tank legs. The u_r, u_i, and u_c are displacements of the rigid mass, impulsive mass, and convective mass, respectively. To obtain the structural parameters of the coupled tank-fluid system the small amplitude linearised fluid surface vibrations theory is considered. These parameters are written as follows [7,8,39],

$$m_{i1} = \gamma_{i1} m_l \tag{4}$$

$$m_{c1} = \left[\frac{2m_l}{(\lambda_1^2 - 1)\lambda_1 S}\right] tanh(\lambda_1 S) \tag{5}$$

$$m_l = \pi R_t^2 H_l \rho_w \tag{6}$$

$$\omega_{i1} = \frac{\phi}{H_l}\sqrt{\frac{E_t g}{\gamma_t}} \tag{7}$$

$$\omega_{c1} = \sqrt{\lambda_1 \frac{g}{R_t} \tanh\left(\lambda_1 S\right)} \tag{8}$$

$$S = \frac{H_l}{R_t} \tag{9}$$

$$k_{i1} = m_{i1}\omega_{i1}^2 \tag{10}$$

$$k_{c1} = m_{c1}\omega_{c1}^2 \tag{11}$$

$$c_{i1} = 2\zeta_{i1} m_{i1} \omega_{i1} \tag{12}$$

$$c_{c1} = 2\zeta_{c1} m_{c1} \omega_{c1} \tag{13}$$

The rigid mass is formulated as the below equation,

$$m_r = m_l - (m_{i1} + m_{c1}) \tag{14}$$

Assuming the rigid mass as shown in Fig. 2 displaces rigidly and the columns connecting the rigid mass to the ground behave as clamped–clamped columns representing a shear behaviour, the stiffness of the columns is written as below,

$$k_r = \frac{12 E_t I_{leg}}{H_{leg}^3} \tag{15}$$

for the thin tubular cross-section of the legs,

$$I_{leg} = \pi R_{leg}^3 t_{leg} \tag{16}$$

while the circular frequency of the vibration of the columns and their corresponding damping coefficient according to the structural dynamics can be conveniently written as follows,

$$\omega_r = \sqrt{\frac{k_r}{m_r}} \tag{17}$$

$$c_r = 2\zeta_r m_r \omega_r \tag{18}$$

which λ_1 is the first root of the first derivative of the Bessel function of the first kind of order one (J_1) and is equal to 1.8412. E_t is the modulus of elasticity of the tank and legs' material, ρ_w is the mass density of the fluid (water), γ_t is the density of the tank material, H_l is the height of the liquid in the tank, g is the gravitational acceleration, S is the aspect ratio, R_t is the radius of the tank, R_{leg} is the radius of the tank's legs, H_{leg} is the height of legs, t_w is the thickness of the tank wall, t_{leg} is the thickness of the tank's legs, ϕ is the Frequency Parameter, and m_l is the total mass of the fluid in the tank. The frequency parameter depends on several factors, most importantly aspect ratio (S), the ratio of the thickness of the wall to the radius of the tank ($\frac{t_w}{R_t}$), and material properties of the tank. Charts have been presented in the literature and seismic design codes for fluid storage tanks to calculate this parameter [8,13,39]. The m_{i1} and m_{c1} are the masses of the first impulsive and the first convective modes, and k_{i1}, k_{c1}, c_{i1}, c_{c1}, ζ_{i1}, ζ_{c1}, ω_{i1}, ω_{c1} are the stiffness, damping coefficients, damping ratios, and circular natural frequencies of these modes, respectively. The ζ_r, and ω_r represent the damping ratio and the natural circular frequency of the legs connecting the rigid mass of the tank to the ground. The

parameters ϕ and γ_{i1} as functions of S for the case of $(\frac{t_w}{R_t}) = 0.004$ can be conveniently obtained from the below equations [40],

$$\phi = 0.037085 + 0.084302S - 0.05088S^2 + 0.012523S^3 - 0.0012S^4 \quad (19)$$

$$\gamma_{i1} = -0.15467 + 1.21716S - 0.62839S^2 + 0.14434S^3 - 0.0125S^4 \quad (20)$$

The state-space representation of Eq. (1) can be formulated according to Eq. (21) which represents a sixth-order dynamical system,

$$\dot{X} = AX + Bu^* \quad (21)$$

where the state and control input matrices A and B are defined as follows,

$$A = \begin{bmatrix} 0 & 1 & 0 & 0 & 0 & 0 \\ -\frac{k_r+k_i+k_c}{m_r} & -\frac{c_r+c_i+c_c}{m_r} & \frac{k_i}{m_r} & \frac{c_i}{m_r} & \frac{k_c}{m_r} & \frac{c_c}{m_r} \\ 0 & 0 & 0 & 1 & 0 & 0 \\ \frac{k_i}{m_i} & \frac{c_i}{m_i} & -\frac{k_i}{m_i} & -\frac{c_i}{m_i} & 0 & 0 \\ 0 & 0 & 0 & 0 & 0 & 1 \\ \frac{k_c}{m_c} & \frac{c_c}{m_c} & 0 & 0 & -\frac{k_c}{m_c} & -\frac{c_c}{m_c} \end{bmatrix},$$

$$B = \begin{bmatrix} B_1 & B_2 \end{bmatrix} \quad (22)$$

$$B_1 = \begin{bmatrix} 0 \\ -\frac{1}{m_r} \\ 0 \\ 0 \\ 0 \\ 0 \end{bmatrix}, B_2 = \begin{bmatrix} 0 \\ -1 \\ 0 \\ -1 \\ 0 \\ -1 \end{bmatrix} \quad (23)$$

while the vectors of states and the control inputs are expressed as,

$$X = \begin{bmatrix} x_1 \\ x_2 \\ x_3 \\ x_4 \\ x_5 \\ x_6 \end{bmatrix} = \begin{bmatrix} u_r \\ \dot{u_r} \\ u_i \\ \dot{u_i} \\ u_c \\ \dot{u_c} \end{bmatrix}, u^* = \begin{bmatrix} f_{MR} \\ \ddot{u_g} \end{bmatrix} \quad (24)$$

It is assumed that the absolute accelerations of the system through accelerometers at the locations of rigid mass, impulsive mass, convective mass, as well as the displacement of the rigid mass are measured. Regarding the mentioned measurements, the output equation for the controlled system is formulated according to Eq. (25),

$$Y = C^*X + Du^* + \epsilon \quad (25)$$

where Y is the output vector and ϵ is the measurement noise. The measurement and direct transition matrices, C^* and D are obtained from Eqs. (26)–(27),

$$C^* = \begin{bmatrix} -\frac{k_r+k_i+k_c}{m_r} & -\frac{c_r+c_i+c_c}{m_r} & \frac{k_i}{m_r} & \frac{c_i}{m_r} & \frac{k_c}{m_r} & \frac{c_c}{m_r} \\ \frac{k_i}{m_i} & \frac{c_i}{m_i} & -\frac{k_i}{m_i} & -\frac{c_i}{m_i} & 0 & 0 \\ \frac{k_c}{m_c} & \frac{c_c}{m_c} & 0 & 0 & -\frac{k_c}{m_c} & -\frac{c_c}{m_c} \end{bmatrix},$$

$$D = \begin{bmatrix} D_1 & D_2 \end{bmatrix} \quad (26)$$

$$D_1 = \begin{bmatrix} -\frac{1}{m_r} \\ 0 \\ 0 \end{bmatrix}, D_2 = [0]_{3\times 1} \quad (27)$$

The MR damper force is calculated based on the modified Bouc–Wen hysteresis dynamic representation of the behaviour of this damper. According to this dynamic modelling, the force produced by the damper is formulated using Eqs. (28)–(33) [42–45],

$$f_{MR} = \alpha z + c_0(\dot{x}_M - \dot{y}) + k_0(x_M - y) + k_1(x_M - x_0) \quad (28)$$

$$\dot{z} = -\gamma|\dot{x}_M - \dot{y}|z|z|^{(n-1)} - \beta(\dot{x}_M - \dot{y})|z|^n + A(\dot{x}_M - \dot{y}) \quad (29)$$

$$\dot{y} = \frac{1}{c_0 + c_1}\left[\alpha z + c_0\dot{x}_M + k_0(x_M - y)\right] \quad (30)$$

$$\alpha(\tau) = \alpha_a + \alpha_b\tau \quad (31)$$

$$c_1(\tau) = c_{1a} + c_{1b}\tau \quad (32)$$

$$c_0(\tau) = c_{0a} + c_{0b}\tau \quad (33)$$

where α_a, α_b, c_{1a}, c_{1b}, c_{0a}, c_{0b}, μ, k_0, k_1, A, β, γ, x_0, and n are the 14 parameters associated with the modified Bouc–Wen model, and x_M and $\dot{x}_M$ are the displacement and velocity of the MR damper. τ is a first-order filter with a transfer function in the s-domain expressed in Eq. (34) that is applied over the decided voltage υ to the damper,

$$\tau(s) = \frac{\mu}{s + \mu} \quad (34)$$

3. Semi-active vibration control techniques

In this study, it is assumed that only the absolute accelerations of the system are measured for the control system design of the coupled fluid-tank system. Thus, acceleration feedback control schemes that rely only on these structural responses are adopted to satisfy the control objectives. Three different control techniques including H2/Linear Quadratic Gaussian (LQG) regulator, Proportional–Integral–Derivative (PID), and Fractional order PID (FOPID) also known as $PI^{\lambda_s}D^{\mu_s}$ in literature [52,57], have been selected in this study to examine the performance of the added semi-active control mechanism to the fluid tank system. For each control technique, an appropriate control objective has been adopted. Each control technique works based on some parameters that need to be designed for the structure under examination and the input disturbance. In this study, an optimisation strategy known as Hunger Game Search (HGS) that has proved to surpass other mostly applied approaches in the literature [54] has been employed to select the optimal values for the parameters of each controller. Finally, as the decided desired control force cannot be commanded due to the nature of the control mechanism a secondary controller is applied to regulate the input voltage to the damper at each time step depending on the requirements of the system to counteract the external disturbances and minimise the vibrations. The Clipped-Optimal Control (COC) scheme [29,55] has been adopted to acquire the command signal to the damper. Thus, three semi-active control strategies, i.e. H2/LQG-COC-HGS, PID-COC-HGS, and FOPID-COC-HGS would be employed. The primary and secondary controllers and the optimisation technique are discussed in the next sections.

3.1. H2/LQG control technique

The H2/Linear Quadratic Gaussian (H2/LQG) control scheme which minimises the H_2 norm of the closed-loop system is an optimal and robust control strategy that has proved efficient in structural vibration control applications [34,44,46–49,58]. Based on the selected control scheme, the desired optimal control force would be obtained using Eq. (35),

$$U_{LQG} = -K_{LQR}\tilde{X} \quad (35)$$

where $\tilde{X}$ is the vector of estimated states using the Kalman-Bucy filter [59–61], and K_{LQR} is the state feedback gain matrix which minimises the infinite horizon linear quadratic cost function with output weighting stated in Eq. (36),

$$J = \lim_{T\to\infty}\frac{1}{T}E\int_0^T (Y^TQY + U_{LQG}^TRU_{LQG})\,dt \quad (36)$$

In this equation, Q and R are weighting matrices that weight selected measured responses of the system and control force, respectively. Solving for P and Θ in the reduced-matrix Riccati Eqs. (37) and (40) gives the gain matrices K_{LQR} of the Linear Quadratic Regulator (LQR) and the K_{LQG} of Kalman filter gain as in Eqs. (39) and (41), respectively,

$$A^T P+PA+C^{*T}QC^{*}-(PB+C^{*T}QD_1)(D_1^TQD_1+R)^{-1}(B_1^TP+D_1^TQC^{*})=0 \tag{37}$$

$$R_s = D_1^T Q D_1 + R \tag{38}$$

$$K_{LQR} = R_s^{-1}(B^T P + D_1^T Q C^{*}) \tag{39}$$

$$A\Theta + \Theta A^T - (C^{*}\Theta)^T(C^{*}\Theta) + B_2 \Lambda B_2^T = 0 \tag{40}$$

$$K_{LQG} = \Theta C^{*T} \tag{41}$$

where Λ represents the power ratio of the process noise to the measurement noise given by,

$$\Lambda = \frac{P(\ddot{u}_g \ddot{u}_g)}{P(\epsilon\epsilon)} \tag{42}$$

where $P(\ddot{u}_g\ddot{u}_g)$ and $P(\epsilon\epsilon)$ are the average power of the signal and noise, respectively. The observer-controller transfer function of the system is represented in the closed form of Eq. (43),

$$K_{Ob-Co}(s) = K_{LQR}(sI-(A-K_{LQG}C^{*}))^{-1}\begin{bmatrix} K_{LQG} & B_1 - K_{LQG}D_1 \end{bmatrix} \tag{43}$$

where B_1 and D_1 are the first columns of matrices B and D, respectively. The Matrix Q was regarded to equally weigh the accelerations of the lumped masses while the parameter R weighs the control effort. The weighting matrix Q, the parameter R, and the Λ are written as follows,

$$Q = \begin{bmatrix} Q_f & 0 & 0 \\ 0 & Q_f & 0 \\ 0 & 0 & Q_f \end{bmatrix}, R = R_f \tag{44}$$

where the parameters Q_f and R_f are optimally designed using the HGS optimisation approach and an adopted objective function. For the H2/LQG-COC-HGS controller, the objective function in the optimisation process of finding the controller's parameters is defined as follows,

$$Obj = \begin{cases} Min\{u_i\}, & |U_{LQG}| < f_{MR,Max} \\ Min\{\ddot{u}_i\}, & |U_{LQG}| \geq f_{MR,Max} \end{cases} \tag{45}$$

Considering the value of the desired control force compared to the capacity of the MR damper, the objective function Obj switches between minimising the displacement or acceleration of the impulsive mass to avoid applying excessive damping forces that could increase the accelerations of the system unnecessarily.

3.2. PID controller

The PID control strategy is one of the widely applied control techniques for various applications. This control strategy has proved to be simple, robust, effective, and applicable to a broad class of industrial systems [62,63]. This technique has been used for control design of industrial processes [64], robotic manipulators [65,66], biomedical applications [67,68], electric drives and power applications [69], and mechanical and civil engineering structures [50,51], to name but a few.

The PID control force in the parallel form is written as below,

$$U_{PID}(t) = K_P\left[e(t) + \frac{1}{T_i}\int_0^t e(t)\,dt + T_d\frac{de(t)}{dt}\right] \tag{46}$$

where $e(t)$ is the error function defined as the difference between the output and the reference. The Laplace transform of the above equation would be as follows,

$$U_{PID}(s) = U_P(s) + U_I(s) + U_D(s) \tag{47}$$

and the controller gain would be,

$$K_{PID}(s) = K_P + \frac{K_P}{T_i}(\frac{1}{s}) + K_P T_d s \tag{48}$$

Considering the below relations,

$$K_I = \frac{K_P}{T_I}, K_D = K_P T_d \tag{49}$$

Eqs. (46) and (48) can be rewritten as Eqs. (50) and (51), respectively,

$$U_{PID}(t) = K_p e(t) + K_i\int_0^t e(t)\,dt + K_d\frac{de(t)}{dt} \tag{50}$$

$$K_{PID}(s) = K_P + K_I(\frac{1}{s}) + K_D s \tag{51}$$

where K_p, K_i, K_d, T_i, T_d, and $e(t)$ are the proportional gain, integral gain, derivative gain, integral time constant, derivative time constant, and the error between the reference and the output, respectively. Since the process usually contains noise, a low-pass filtered derivative instead of the pure derivative is applied. In this case, the control force in Eq. (52) would be reformulated as follows,

$$U_{PID}(s) = U_P(s) + U_I(s) + U_{D-LPF}(s) \tag{52}$$

where the filtered derivative term would be in the below form,

$$U_{D-LPF} = K_D\left[\frac{s}{T_f s+1}\right] \tag{53}$$

where T_f is the filter time constant.

3.3. FOPID controller

Fractional controllers that are indeed based on the fractional calculus were developed for controlling dynamical systems [70]. Fractional order PID (FOPID) introduced by Podlubny [57] is indeed a generalised form of PID controller which depending on the values of the parameters could reduce to different forms of Proportional (P), Proportional–Integral (PI), Proportional–Derivative (PD), PID, and finally the general form of $PI^{\lambda_s}D^{\mu_s}$. FOPID controllers through having non-integer orders for the derivation and integration processes try to enhance the performance of the PID controllers [45,52,53]. In this controller, contrary to the PID controller, a generalised operator which is the extended form of integration and differentiation is applied. The fractional order calculus is defined by the below equation,

$$D_t^{\Phi} = \begin{cases} \frac{d^{\Phi}}{dt^{\Phi}} & \Phi > 0 \\ 1 & \Phi = 0 \\ \int_0^t (d\tau)^{\Phi} & \Phi < 0 \end{cases} \tag{54}$$

Thus, the control force and the controller gain based on this control law can be obtained from the below equations, respectively,

$$U_{FOPID}(t) = K_P e(t) + K_I D^{-\lambda_s} e(t) + K_D D^{\mu_s} e(t) \tag{55}$$

$$K_{FOPID}(s) = K_P + \frac{K_I}{s^{\lambda_s}} + K_D s^{\mu_s}, (\lambda_s, \mu_s > 0) \tag{56}$$

where λ_s and μ_s are the non-integer orders of the integration and derivation processes, respectively.

3.4. Error-based objective function

When designing or optimising the PID and FOPID control parameters one efficient methodology is to use some error criteria instead of the error function itself [71]. Different error performance indices have been proposed in the literature for this purpose including Integral of time-weighted absolute error (ITAE), Integral of squared error (ISE), Integral of absolute error (IAE), Integral of time-weighted squared error (ITSE), Integral of squared time-weighted squared error (ISTSE), and Integral of squared time-weighted error (ISTE) [52,71–74]. In this study,

the ITAE error-based performance index criterion which has proved powerful features including smaller overshoots and oscillations, less settling time, no steady-state error, and computational efficiency [52,71], is adopted as the objective function for the optimisation process of the HGS algorithm. This error criterion is defined as follows,

$$ITAE = \int_0^\infty t|e(t)|\,dt \tag{57}$$

Since among the three lumped masses the acceleration of the impulsive mass is the greatest, hence the error function for both PID-COC-HGS and FOPID-COC-HGS controllers is defined as the difference between the reference and the impulsive mass acceleration as below,

$$e(t) = \ddot{u}_{ref} - \ddot{u}_i \tag{58}$$

$$\ddot{u}_{ref} = 0 \rightarrow e(t) = -\ddot{u}_i \tag{59}$$

3.5. Secondary controller

Finally, the control signal using the secondary controller would be acquired using Eq. (60) [29,44,55,56],

$$v_{MR} = V_{max,MR} H\{(U_{Cont} - f_{MR}) f_{MR}\} \tag{60}$$

where $V_{max,MR}$ is the maximum voltage that can be commanded to the damper which depends on the capacity and specifications of the damper, $H\{.\}$ is the Heaviside function, and U_{Cont} is the desirable control force decided by the selected control laws and strategies.

4. Hunger Game Search optimisation

A variety of optimisation techniques have been proposed in the literature for the purpose of selecting the optimal and best values of parameters that affect the minimum value of a cost or objective function in engineering problems [75–77]. Most of the optimisation strategies used in the literature so far mainly focused on two major ideas, i.e. evolution and swarm intelligence. Examples of such tactics include the Genetic Algorithm (GA) [78], Particle Swarm Optimisation (PSO) [79], Ant Colony Optimisation (ACO) [80], Harris Hawk Optimiser (HHO) [81], Grey Wolf Optimiser (GWO) [82], etc. The Hunger Game Search (HGS) recently developed by Yang et al. [54] is indeed a general-purpose optimisation approach which is a population-based method. This dynamic technique is based on hunger as the most crucial desire in all animals for decision-making. It follows some logical rules called "games", has a simple structure, has proved promising features including stability and competitive performance, and has been validated for benchmark and IEEE CEC2014 functions [54]. Considering the main concept of this method, three rules (games) are applied as follows [54],

$$\overrightarrow{X(t+1)} = \begin{cases} \text{Game 1} & : \textit{search based on } \overrightarrow{X(t)} \\ \text{Games 2 and 3} & : \textit{search based on } \overrightarrow{X_b} \end{cases} \tag{61}$$

where t is the current iteration. In *Game* 1 there is a set of instructions for finding the food without any teamwork and only based on each individual's location ($\overrightarrow{X(t)}$) and does not include any cooperative communication. On the other hand, Games 2 and 3 are based on cooperation between search agents for finding the food using some functions termed "weights of hunger", and the best individual's location ($\overrightarrow{X_b}$) in each iteration. These games and their weights are represented using mathematical rules and fitness functions for the search methodology for the location of agents to guarantee the optimal solution. The mathematical details of this technique can be found in [54] and are not discussed here for brevity. The schematic of the control design block diagram has been illustrated in Fig. 3.

Table 1
Parameters of the Bouc–Wen model of the MR damper.

Parameter	Value	Parameter	Value
α_a	1921.141 (N/m)	k_0	1940.405 (N/m)
α_b	5882.51 (N/V m)	k_1	1.751268 (N/m)
c_{1a}	2089.263 (N s/m)	A	155.32
c_{1b}	14384.918 (N s/V m)	β	36332.07 (m^{-2})
c_{0a}	651.4718 (N s/m)	γ	36332.07 (m^{-2})
c_{0b}	1043.7559 (N s/V m)	x_0	0.00 (m)
μ	60 (s^{-1})	n	2

5. Simulations and results

To investigate the efficacy of MR dampers in vibration mitigation of the fluid-tank system shown in Fig. 1, an example of a stainless-steel circular cylindrical tank with a height of 1500 mm, a radius of 425 mm, and a shell thickness of 1.7 mm is considered. Legs are stainless-steel pipes with a thickness of 2 mm, height of 795 mm, and radius of 50 mm. Other specifications of the tank are modulus of elasticity, $E_t = 200$ GPa, poison's ratio $\nu = 0.3$, density of steel, $\rho_s = 7850$ kg/m^3, and density of water, $\rho_w = 1000$ kg/m^3. Damping ratios of 2% and 0.5% have been considered for the tank shell material and the convective modes of fluid vibrations. The damping ratio for legs has been regarded as similar to that of the shell body. This fluid-tank system has been modelled by considering the first fundamental impulsive mode and the first fundamental convective mode to represent the fluid–structure interaction between the tank shell and the fluid domain. The parameter Λ for the noise process of the H2/LQG control technique was selected as 50.

The considered MR damper in this study has a capacity of around 2.45 KN, and the input voltage to the damper is regarded in the range of 0 to 5 V. The MR damper model regarded in this study is RD-8041-1 (long stroke). The parameters of the modified Bouc–Wen model for the MR damper are considered as presented in Table 1 which have been experimentally obtained and verified in previous investigations (Gao, 2012). The fluid-tank-MR system has been studied under six seismic events, three Far-Fault, and three Near-Fault, as shown along with their characteristics in Table 2. In this table, M_w is the moment magnitude of the earthquake, PGA is the Peak Ground Acceleration in g (gravitational acceleration), and DF is the dominant frequency of the record in Hz. The frequency content of the selected input ground motions to examine the performance of the equipped fluid tank with the MR damper is shown in Fig. 4. In this figure, $|P1(f)|$ is the single-sided amplitude spectrum of the signal versus the Nyquist frequencies, in the frequency domain f (Hz), calculated using the signal processing toolbox of MATLAB R2023b. The coupled tank-liquid-MR damper system was analysed under uncontrolled and five different control strategies, including three semi-active and two passive control strategies. A description of the applied control techniques and their designed parameters using the HGS optimisation method for each ground motion and aspect ratio have been presented in Table 3.

Numerical simulations have been conducted using SIMULINK and MATLAB R2023b to calculate the vibrational responses of the system under the considered ground motion. Results have been compared for different scenarios of the control strategies and aspect ratios as the main operational condition to evaluate the efficacy of the added damper to the fluid tank system. These scenarios include the uncontrolled case, the controlled system with three different control techniques including H2/LQG-COC-HGS, PID-COC-HGS, and FOPID-COC-HGS controllers, as well as two other scenarios in which the MR damper has been regarded merely as a passive device that requires no control signal to be commanded at each time step. These passive modes are the Passive Off and the Passive On modes in which the voltage to the damper has been held at 0 V and the maximum level of 5 V throughout the control process, respectively. Table 4 shows the peak structural responses of the system under these scenarios. In this table, $\ddot{u}_{r,i,c}$ represent the peak absolute

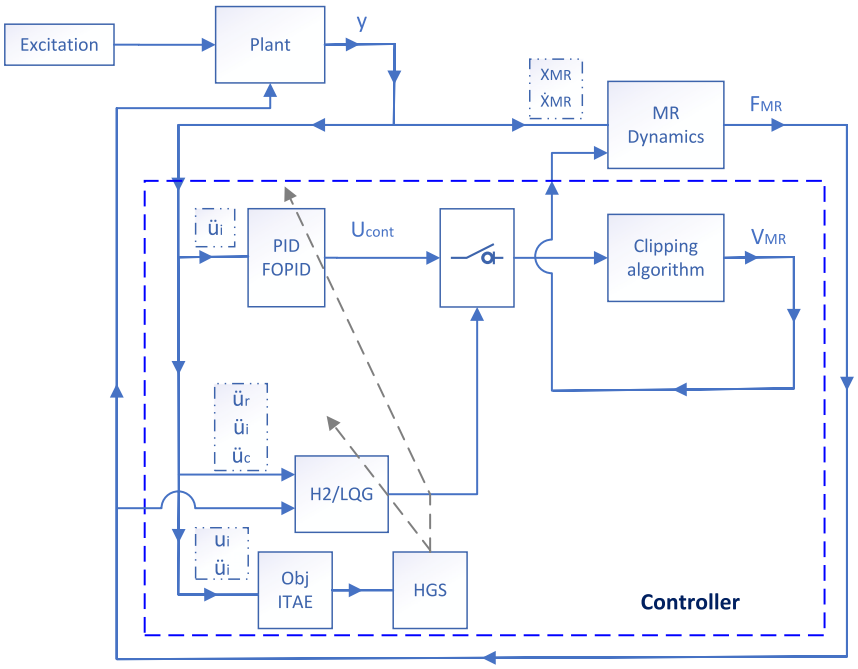

Fig. 3. Schematic of the control design block diagram.

Table 2
Characteristics of the selected input ground motions.

Event	Year	Fault type	M_w	PGA (g)	DF (Hz)
El Centro	1940	Far-Fault	6.9	0.348	7.32
Hachinohe	1968	Far-Fault	7.8	0.229	1.83
Kobe	1995	Near-Fault	6.9	0.833	7.26
Northridge	1994	Near-Fault	6.7	0.842	3.17
Manjil	1990	Far-Fault	7.37	0.497	9.58
Tabas	1978	Near-Fault	7.35	0.854	6.35

accelerations of each mass, $u_{r,i,c}$ are the peak relative displacements, f_{MR}^{max} is the peak generated force by the MR damper corresponding to each control strategy, f_{i1} the first cyclic impulsive frequency, and f_{c1} is the first cyclic convective frequency.

It can be seen from Table 4 that the MR damper has reduced the vibrational response of the fluid tank system in all considered control scenarios. Reductions in responses of the convective mass are not considerable which could be justified by the very different vibrational properties (frequency and stiffness) of this mode from the impulsive and rigid modes. In fact, even though the damper has caused a substantial decrease in the structural responses of the rigid and impulsive modes, the significant difference between the stiffness and the damping of the convective mode from the other two modes has caused the damper to have little effects on its vibrational responses. It is noteworthy that the far too different vibrational properties of the convective mass cause its structural responses to be far away less affected by the responses of the other two modes even without having the damper in place which is evident from Table 4. It should be noted that for the three aspect ratios of $S = 1$, 2, and 3, the impulsive mass contributes to between 57%–73% of the total mass of the system, and hence its vibrational responses are the governing ones for the analysis and design purposes.

To evaluate the performance of the applied control strategies in reducing the seismic structural responses of the coupled fluid-tank-MR system, four performance indices ($PI's$), termed as PI_1 to PI_4 are defined. These $PI's$ represent the ratios of the peak absolute structural responses in the controlled case to the uncontrolled one. These $PI's$ are considered as follows,

$$PI_1 = \frac{Max|u_{r,co}|}{Max|u_{r,uco}|} \tag{62}$$

$$PI_2 = \frac{Max|\ddot{u}_{r,co}|}{Max|\ddot{u}_{r,uco}|} \tag{63}$$

$$PI_3 = \frac{Max|u_{i,co}|}{Max|u_{i,uco}|} \tag{64}$$

$$PI_4 = \frac{Max|\ddot{u}_{i,co}|}{Max|\ddot{u}_{i,uco}|} \tag{65}$$

where $u_{r,i,co}$, $\ddot{u}_{r,i,uco}$, are the controlled and uncontrolled rigid and impulsive relative displacements and absolute accelerations, respectively. These performance indices have been calculated for the considered ground motions, control strategies, and each aspect ratio as shown in Table 5.

Examining the structural responses in Table 4 and the performance indices in Table 5 shows that for the aspect ratio of 1 the highest reductions in the structural responses including the lateral displacements and absolute accelerations of the rigid and impulsive mass in the controlled case occur under the Tabas earthquake followed by the El Centro earthquake. However, for the aspect ratio of 2 the least responses of the controlled system are achieved under the El Centro earthquake followed by the Manjil earthquake. For the aspect ratio of 1, depending on the applied control technique, reductions up to around 71% in the lateral displacements of the rigid and impulsive mass and up to 65% in the absolute accelerations of these masses have been achieved. For the aspect ratio of 2, these reductions are further increased by a few percentage points. For the considered ground motions except for the Tabas earthquake, by increasing the aspect ratio from 1 to 2, further reductions in the peak lateral displacements and absolute accelerations of the rigid and impulsive masses in the case of Passive On and semi-active control strategies can be found. For all aspect ratios and

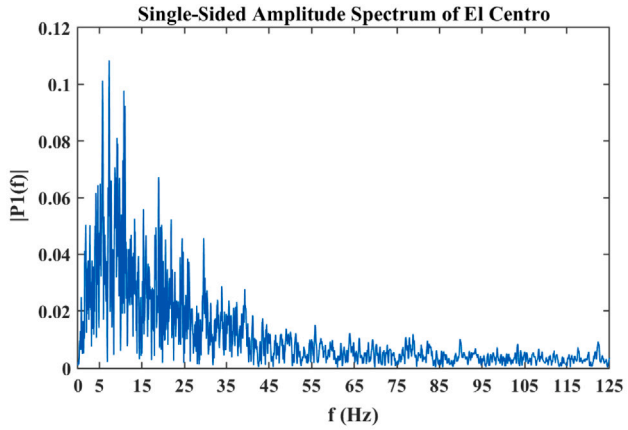

(a) ElCentro

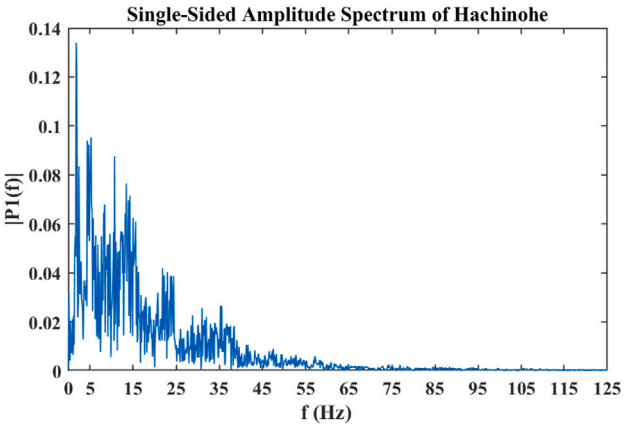

(b) Hachinohe

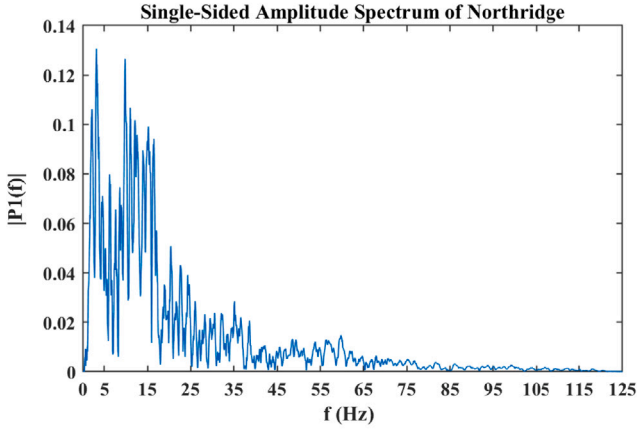

(c) Northridge

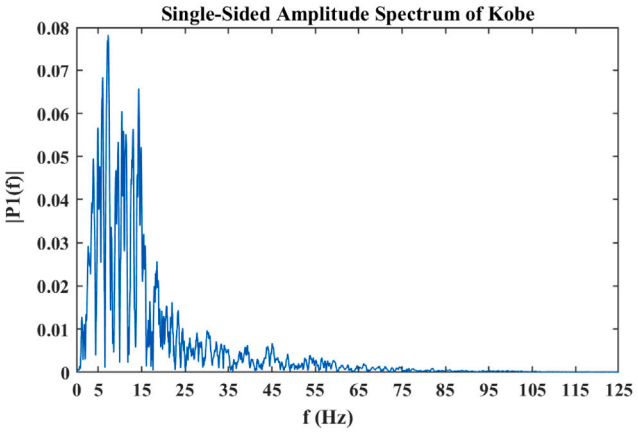

(d) Kobe

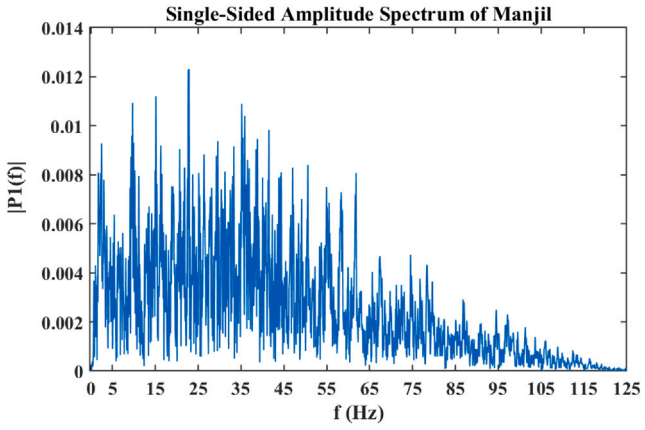

(e) Manjil

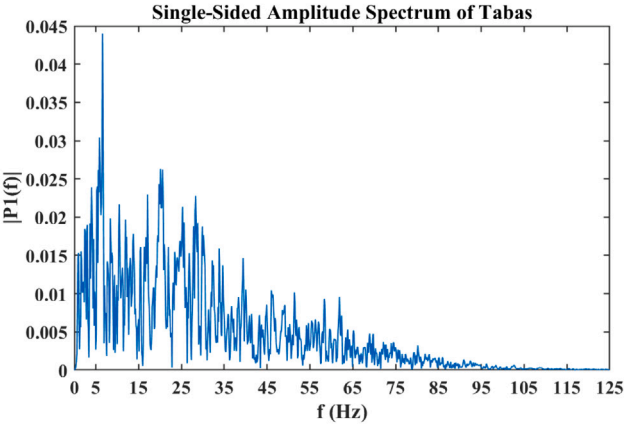

(f) Tabas

Fig. 4. Frequency content of the selected Far-Fault and Near-Fault ground motions.

under all the applied ground motions, the responses of the impulsive mass in the uncontrolled case, are higher than that of the rigid mass. Utilising the MR damper as the smart control mechanism and the semi-active control techniques applied in this study considerably reduce the structural responses of these two masses. The lateral displacements and absolute accelerations of the rigid and impulsive mass of the controlled system closely follow each other. For the aspect ratio of 3, the reductions in the lateral displacements and absolute accelerations of

Table 3
Optimal parameters of the selected semi-active controllers.

Controller	Objective	Parameters	Range	El Centro	Hachinohe	Kobe	Northridge	Manjil	Tabas
			$S = 1.00$ (*Broad tank*)						
PID-COC-HGS	ITAE	K_P	$[0\ 25000] \in \mathbb{R}$	25 000	25 000	0.00	19 483	1891.90	11 587
		K_I	$[0\ 25000] \in \mathbb{R}$	23 033.60	24 419	0.00	0.00	24 989	24 318
		K_D	$[0\ 10^4] \in \mathbb{R}$	2691.50	1857	9345.50	631.60	7913.60	5986.50
FOPID-COC-HGS	ITAE	K_P	$[0\ 10^4] \in \mathbb{R}$	10 000	0.00	336.70	9464.50	9077.20	9631.40
		K_I	$[0\ 10^4] \in \mathbb{R}$	868.20	4501.50	4186.90	1.146	5951.10	2545.90
		K_D	$[0\ 10^4] \in \mathbb{R}$	6416.60	10 000	1527.80	10 000	1397	7481.10
		λ_s	$[0\ 2] \in \mathbb{R}$	0.00	0.96	0.83	2.00	1.30	0.10
		μ_s	$[0\ 2] \in \mathbb{R}$	0.56	0.50	0.59	0.47	0.64	0.59
H2/LQG-COC-HGS	*Obj*	Q_f	$[0\ 1] \in \mathbb{R}$	0.7813	0.9279	0.7883	0.8853	0.4172	0.5386
		R_f	$[10^{-1}\ 10^{-16}] \in \mathbb{R}$	$10^{-3.77}$	10^{-4}	$10^{-8.76}$	$10^{-3.57}$	$10^{-3.91}$	$10^{-3.81}$
			$S = 2.00$ (*Slender tank*)						
PID-COC-HGS	ITAE	K_P	$[0\ 25000] \in \mathbb{R}$	25 000	22 011	14 604	15 499	25 000	25 000
		K_I	$[0\ 25000] \in \mathbb{R}$	2228.50	1663	23 119	2818	389.84	0.00
		K_D	$[0\ 10^4] \in \mathbb{R}$	1369.60	2272	899.94	882.84	2550.30	3120
FOPID-COC-HGS	ITAE	K_P	$[0\ 10^4] \in \mathbb{R}$	0.00	1781.30	9505.70	1428.70	4005.10	10 000
		K_I	$[0\ 10^4] \in \mathbb{R}$	7852.94	0.00	2662.30	10 000	1427.40	4020.90
		K_D	$[0\ 10^4] \in \mathbb{R}$	6434	5134.50	9968.70	3547.90	1418.20	9008.80
		λ_s	$[0\ 2] \in \mathbb{R}$	1.01	0.1211	2.00	1.29	0.75	2.00
		μ_s	$[0\ 2] \in \mathbb{R}$	0.44	0.4895	0.53	0.46	0.51	0.53
H2/LQG-COC-HGS	*Obj*	Q_f	$[0\ 1] \in \mathbb{R}$	0.6053	0.8036	0.7388	1.00	0.7959	0.8279
		R_f	$[10^{-1}\ 10^{-16}] \in \mathbb{R}$	$10^{-4.67}$	$10^{-4.47}$	$10^{-4.63}$	$10^{-4.36}$	$10^{-4.45}$	$10^{-4.49}$
			$S = 3.00$ (*Slender tank*)						
PID-COC-HGS	ITAE	K_P	$[0\ 25000] \in \mathbb{R}$	24 260	17 193	16 061	17 687	25 000	25 000
		K_I	$[0\ 25000] \in \mathbb{R}$	284	8411	0.00	14 203	11 464	2180
		K_D	$[0\ 10^4] \in \mathbb{R}$	825	659	814.60	758.70	997.66	1215.50
FOPID-COC-HGS	ITAE	K_P	$[0\ 10^4] \in \mathbb{R}$	9998.50	2208.70	59.62	5591.30	7845.02	3373.10
		K_I	$[0\ 10^4] \in \mathbb{R}$	2265	8119.80	4908.52	0.00	4799.40	10 000
		K_D	$[0\ 10^4] \in \mathbb{R}$	10 000	5916.10	7922.06	7930.80	7899.20	9055.10
		λ_s	$[0\ 2] \in \mathbb{R}$	1.20	1.06	0.00	2.00	0.45	0.93
		μ_s	$[0\ 2] \in \mathbb{R}$	0.47	0.46	0.50	0.46	0.47	0.48
H2/LQG-COC-HGS	*Obj*	Q_f	$[0\ 1] \in \mathbb{R}$	0.3104	0.9490	1.00	0.020	0.0447	0.3344
		R_f	$[10^{-1}\ 10^{-16}] \in \mathbb{R}$	$10^{-5.42}$	$10^{-4.71}$	$10^{-4.75}$	$10^{-6.64}$	$10^{-6.27}$	$10^{-5.32}$

the rigid and impulsive mass under all seismic events and the employed control techniques become much closer to each other. For this aspect ratio, reduction percentage points in the lateral displacements of the rigid and impulsive mass using different semi-active control strategies and under the applied ground motions range between 54.7% for the rigid mass under the Hachinohe earthquake using the FOPID-COC-HGS to 17.5% for the impulsive mass under the Tabas earthquake using the H2/LQG-COC-HGS control technique. For all control techniques, applied earthquakes, and considered aspect ratios of the fluid tank, the least reductions in the controlled case occur under the Northridge earthquake for the aspect ratio of 1 which is reflected in PI_2 index. Decreases in the peak lateral displacements and absolute accelerations of the rigid and impulsive masses almost follow the same trends and reduction percentage points. Among the considered semi-active control strategies, PID-COC-HGS and FOPID-COC-HGS have contributed to the most reductions in the structural responses, followed by Passive On mode. However, reductions in the case of Passive On would be at the expense of having the voltage commanded through the whole process. As apparent from the results of Tables 4 and 5 and shown in Figs. 5–16 the PID-COC-HGS and FOPID-COC-HGS control techniques have made the most reductions in the structural responses and surpassed the H2/LQG-COC-HGS. These two control strategies almost make the same reduction percentage points in the peak responses. The designed H2/LQG-COC-HGS control strategy has produced the least MR damper force of around 47%–78% of the corresponding force in the case of the Passive On control strategy for all three aspect ratios for each ground motion. This technique has achieved comparable reductions with a maximum difference of around 23% with other semi-active control techniques, shown in PI_2 for the aspect ratio of 1.

Depending on the aspect ratio, the control scheme, and the applied ground motion, the MR damper has reduced the peak relative displacements of the rigid and impulsive masses up to 72% and a reduction percentage point for the peak absolute accelerations of these masses up to 67% has been achieved. Under the Northridge earthquake, by increasing the aspect ratio of the fluid-tank-MR damper system up to 3, more reductions in the structural responses, comparable to other earthquakes, are observed. For the aspect ratio 1, PI_1 to PI_4 of the control techniques under the Hachinohe and Kobe earthquakes are very close to each other while the performance indices of El Centro and Tabas follow the same trend. For the aspect ratio of 2, similar performance indices can be seen under the Kobe and Northridge for most of the semi-active control techniques. The frequency of the first convective mode by increasing the aspect ratio from 1 to 3 does not change significantly (from 1.01 Hz to 1.04 Hz). However, the frequency of the first impulsive mode changes substantially from 154.68 Hz for the aspect ratio of 1 to 45.99 Hz for the aspect ratio of 3. For the aspect ratio of 3, comparable performance indices for most control techniques and under different earthquakes can be seen except for the Tabas earthquake.

In fluid storage tanks, the base shear and overturning moments contribute to the main causes of damage to these structures under the base excitations. According to Eqs. (66) and (67) the maximum of the base shear and overturning moment using the square root of the sum of squares (SRSS) are related to the peak accelerations of the rigid, impulsive, and convective masses [8,39],

$$Q^b{}_{max} = \sqrt{(m_c S_{a,c})^2 + (m_i S_{a,i})^2 + ((m_i - m_r)\ddot{u}_g^{max})^2} \tag{66}$$

$$M^o{}_{max} = \sqrt{(m_c h_c S_{a,c})^2 + (m_i h_i S_{a,i})^2 + ((m_i h_i - m_r h_r)\ddot{u}_g^{max})^2} \tag{67}$$

Table 4
Peak responses of the tank-liquid-MR damper system under the selected ground motions for different control techniques and aspect ratios.

Response	Control technique	El Centro	Hachinohe	Kobe	Northridge	Manjil	Tabas
		$S = 1.00$ (*Broad tank*), $f_{i1} = 154.68$ Hz, $f_{c1} = 1.01$ Hz					
u_r (cm)	Uncontrolled	0.0122	0.0032	0.0124	0.0125	0.0278	0.0364
	PID-COC-HGS	0.0036	0.0018	0.0069	0.0096	0.0129	0.0107
	FOPID-COC-HGS	0.0037	0.0018	0.0069	0.0097	0.0127	0.0105
	H2/LQG-COC-HGS	0.0048	0.0020	0.0083	0.0110	0.0128	0.0148
	Passive On	0.0036	0.0018	0.0069	0.0094	0.0127	0.0103
	Passive Off	0.0091	0.0030	0.0104	0.0112	0.0236	0.0299
$\ddot{u}_r$ (cm/s^2)	Uncontrolled	1226.42	360.01	1321.62	1270.56	2809.24	3633.07
	PID-COC-HGS	474.68	243.17	850.88	1233.20	1543.45	1300.54
	FOPID-COC-HGS	475.71	243.20	854.12	1238.99	1529.63	1336.64
	H2/LQG-COC-HGS	614.34	265.80	921.37	1221.14	2414.51	2152.96
	Passive On	474.31	243.71	854.90	1219.82	1524.81	1279.12
	Passive Off	920.48	307.76	1128.63	1218.65	2381.67	3004.52
u_i (cm)	Uncontrolled	0.0136	0.0036	0.0139	0.0139	0.0311	0.0407
	PID-COC-HGS	0.0042	0.0021	0.0078	0.0110	0.0147	0.0122
	FOPID-COC-HGS	0.0042	0.0021	0.0079	0.0111	0.0145	0.0120
	H2/LQG-COC-HGS	0.0054	0.0023	0.0092	0.0123	0.0144	0.0168
	Passive On	0.0041	0.0021	0.0079	0.0108	0.0144	0.0118
	Passive Off	0.0102	0.0033	0.0116	0.0125	0.0263	0.0333
$\ddot{u}_i$ (cm/s^2)	Uncontrolled	1336.81	377.08	1380.08	1371.16	3093.86	4025.24
	PID-COC-HGS	519.87	250.11	856.70	1312.34	1712.28	1442.77
	FOPID-COC-HGS	521.07	250.11	860.39	1318.87	1696.88	1428.78
	H2/LQG-COC-HGS	578.55	262.06	933.95	1295.41	1521.22	1846.36
	Passive On	519.95	250.59	861.22	1294.46	1698.13	1409.04
	Passive Off	1009.19	320.23	1165.60	1298.88	2636.32	3261.32
u_c (cm)	Uncontrolled	1.03	1.12	1.44	2.18	3.21	6.66
	PID-COC-HGS	1.03	1.12	1.44	2.18	3.21	6.66
	FOPID-COC-HGS	1.03	1.12	1.44	2.18	3.21	6.66
	H2/LQG-COC-HGS	1.03	1.12	1.44	2.18	3.21	6.66
	Passive On	1.03	1.12	1.44	2.18	3.21	6.66
	Passive Off	1.03	1.12	1.44	2.18	3.21	6.66
$\ddot{u}_c$ (cm/s^2)	Uncontrolled	41.66	45.23	58.16	88.29	130.09	269.45
	PID-COC-HGS	41.68	45.24	58.08	88.49	129.62	268.84
	FOPID-COC-HGS	41.68	45.24	58.08	88.49	129.62	268.84
	H2/LQG-COC-HGS	41.69	45.24	58.08	88.42	129.65	268.85
	Passive On	41.68	45.24	58.08	88.48	129.62	268.84
	Passive Off	41.69	45.24	58.09	88.25	129.77	268.85
f_{MR}^{max} (N)	Uncontrolled	–	–	–	–	–	–
	PID-COC-HGS	193	62	193	427	526	462
	FOPID-COC-HGS	191	61	196	419	535	468
	H2/LQG-COC-HGS	92	37	102	254	288	343
	Passive On	195	63	199	438	549	482
	Passive Off	21	5.9	16	25	60	72
		$S = 2.00$ (*Slender tank*), $f_{i1} = 78.59$ Hz, $f_{c1} = 1.04$ Hz					
u_r (cm)	Uncontrolled	0.0380	0.0134	0.0385	0.0452	0.0932	0.1200
	PID-COC-HGS	0.0106	0.0065	0.0246	0.0272	0.0296	0.0572
	FOPID-COC-HGS	0.0106	0.0065	0.0247	0.0284	0.0298	0.0565
	H2/LQG-COC-HGS	0.0135	0.0091	0.0254	0.0263	0.0356	0.0691
	Passive On	0.0106	0.0065	0.0247	0.0263	0.0293	0.0540
	Passive Off	0.0318	0.0127	0.0356	0.0369	0.0733	0.0951
$\ddot{u}_r$ (cm/s^2)	Uncontrolled	1363.31	479.48	1406.91	1616.96	3379.97	4181.78
	PID-COC-HGS	455.74	306.10	1058.28	1136.27	1231.60	2311.71
	FOPID-COC-HGS	457.16	305.66	1061.00	1168.77	1240.19	2286.06
	H2/LQG-COC-HGS	546.57	367.01	1039.32	1043.78	1350.58	2587.02
	Passive On	454.57	304.43	1064.52	1122.80	1221.42	2211.42
	Passive Off	1124.50	458.21	1313.20	1316.54	2591.94	3420.14
u_i (cm)	Uncontrolled	0.0444	0.0156	0.0449	0.0527	0.1100	0.1400
	PID-COC-HGS	0.0128	0.0078	0.0292	0.0325	0.0355	0.0679
	FOPID-COC-HGS	0.0128	0.0078	0.0293	0.0338	0.0359	0.0672
	H2/LQG-COC-HGS	0.0159	0.0107	0.0300	0.0310	0.0420	0.0813
	Passive On	0.0127	0.0078	0.0293	0.0316	0.0353	0.0642
	Passive Off	0.0372	0.0148	0.0416	0.0431	0.0855	0.1100
$\ddot{u}_i$ (cm/s^2)	Uncontrolled	1538.54	543.81	1571.15	1826.05	3760.97	4755.60
	PID-COC-HGS	524.11	321.69	1120.89	1293.56	1463.17	2620.47
	FOPID-COC-HGS	524.31	320.18	1123.97	1324.45	1473.48	2593.95
	H2/LQG-COC-HGS	598.70	406.05	1125.38	1148.26	1576.60	2963.13
	Passive On	523.29	322.44	1126.11	1277.89	1467.39	2502.39
	Passive Off	1302.25	520.28	1462.24	1503.49	2975.21	3897.05

(*continued on next page*)

Table 4 (*continued*).

Response	Control technique	El Centro	Hachinohe	Kobe	Northridge	Manjil	Tabas
u_c (cm)	Uncontrolled	1.03	0.94	1.63	2.18	3.47	6.19
	PID-COC-HGS	1.03	0.94	1.63	2.18	3.47	6.19
	FOPID-COC-HGS	1.03	0.94	1.63	2.18	3.47	6.18
	H2/LQG-COC-HGS	1.03	0.94	1.63	2.18	3.47	6.18
	Passive On	1.03	0.94	1.63	2.18	3.47	6.14
	Passive Off	1.03	0.94	1.63	2.18	3.48	6.15
$\ddot{u}_c$ (cm/s^2)	Uncontrolled	44.02	40.01	69.38	92.57	148.23	263.58
	PID-COC-HGS	43.51	40.00	69.39	93.21	147.23	262.23
	FOPID-COC-HGS	43.50	40.00	69.37	93.15	147.24	262.21
	H2/LQG-COC-HGS	43.49	40.00	69.40	93.08	147.41	262.04
	Passive On	43.50	40.00	69.38	93.22	147.27	260.33
	Passive Off	43.78	40.06	69.55	92.72	147.94	260.66
f_{MR}^{max} (N)	Uncontrolled	–	–	–	–	–	–
	PID-COC-HGS	444	250	805	911	1110	1496
	FOPID-COC-HGS	443	251	804	796	1111	1514
	H2/LQG-COC-HGS	303	181	541	584	751	1165
	Passive On	449	249	810	984	1126	1486
	Passive Off	62	23	66	71	121	145
	$S = 3.00$ ($Slender\ tank$), $f_{i1} = 45.99$ Hz, $f_{c1} = 1.04$ Hz						
u_r (cm)	Uncontrolled	0.0489	0.0506	0.0782	0.0782	0.0889	0.1300
	PID-COC-HGS	0.0223	0.0230	0.0404	0.0431	0.0459	0.0896
	FOPID-COC-HGS	0.0224	0.0229	0.0404	0.0433	0.0457	0.0899
	H2/LQG-COC-HGS	0.0253	0.0319	0.0452	0.0508	0.0601	0.1000
	Passive On	0.0218	0.0228	0.0402	0.0433	0.0456	0.0892
	Passive Off	0.0423	0.0475	0.0677	0.0701	0.0862	0.1200
$\ddot{u}_r$ (cm/s^2)	Uncontrolled	991.93	1026.61	1571.34	1561.33	1734.08	2505.27
	PID-COC-HGS	522.75	565.66	970.35	1128.05	1046.30	1982.51
	FOPID-COC-HGS	524.37	560.66	972.06	1132.00	1041.52	1989.16
	H2/LQG-COC-HGS	564.46	740.47	992.28	1249.49	1291.23	2260.33
	Passive On	514.79	558.64	968.66	1134.23	1044.94	1971.56
	Passive Off	869.76	971.76	1361.92	1434.88	1720.87	2389.75
u_i (cm)	Uncontrolled	0.0636	0.0659	0.1000	0.1000	0.1200	0.1600
	PID-COC-HGS	0.0306	0.0313	0.0537	0.0580	0.0622	0.1200
	FOPID-COC-HGS	0.0308	0.0312	0.0538	0.0583	0.0620	0.1200
	H2/LQG-COC-HGS	0.0336	0.0423	0.0590	0.0669	0.0795	0.1400
	Passive On	0.0300	0.0310	0.0535	0.0584	0.0617	0.1200
	Passive Off	0.0550	0.0620	0.0882	0.0914	0.1100	0.1600
$\ddot{u}_i$ (cm/s^2)	Uncontrolled	1225.83	1277.95	1964.78	1971.29	2230.01	3179.72
	PID-COC-HGS	695.39	693.06	1113.67	1248.05	1352.41	2506.66
	FOPID-COC-HGS	696.48	687.51	1113.91	1252.55	1355.83	2513.61
	H2/LQG-COC-HGS	693.18	866.87	1157.63	1346.19	1625.76	2738.26
	Passive On	680.47	684.38	1108.57	1260.25	1356.24	2489.80
	Passive Off	1064.36	1205.96	1712.66	1779.60	2164.26	3050.08
u_c (cm)	Uncontrolled	1.02	0.94	1.64	2.18	3.48	6.18
	PID-COC-HGS	1.02	0.94	1.64	2.19	3.48	6.18
	FOPID-COC-HGS	1.02	0.94	1.64	2.18	3.48	6.18
	H2/LQG-COC-HGS	1.02	0.94	1.64	2.18	3.48	6.18
	Passive On	1.03	0.94	1.64	2.18	3.48	6.18
	Passive Off	1.02	0.94	1.64	2.18	3.47	6.19
$\ddot{u}_c$ (cm/s^2)	Uncontrolled	44.42	41.77	69.79	95.55	148.73	263.62
	PID-COC-HGS	43.58	40.77	69.77	94.63	147.69	263.24
	FOPID-COC-HGS	43.43	40.79	69.78	94.63	147.69	263.28
	H2/LQG-COC-HGS	43.52	41.14	69.85	94.88	147.89	263.41
	Passive On	43.65	40.76	69.88	94.62	147.66	263.23
	Passive Off	44.21	41.61	69.63	95.41	148.14	263.34
f_{MR}^{max} (N)	Uncontrolled	–	–	–	–	–	–
	PID-COC-HGS	809	766	1207	1255	1379	1850
	FOPID-COC-HGS	814	766	1203	1235	1381	1849
	H2/LQG-COC-HGS	534	592	842	810	1089	1357
	Passive On	803	765	1207	1266	1380	1957
	Passive Off	67	73	96	98	120	140

where, ${Q^b}_{max}$ and ${M^o}_{max}$ are the maximum base shear and overturning moment, $S_{a,c}$ and $S_{a,i}$ are the spectral accelerations of the fundamental convective and impulsive masses, h_c and h_i are the height of the corresponding masses from the base, respectively, and $\ddot{u}_g^{max}$ is the PGA of the ground motion. It is therefore concluded that the achieved reductions in the peak absolute accelerations of these masses can result in significant reductions of the system's base shear and overturning moments, thus reducing the damage risks in these structures.

6. Conclusions

Various seismic energy-dissipating devices have been introduced in the literature for seismic retrofitting and vibration mitigation of fluid tanks. Most of these devices are passive systems which their characteristics cannot be adapted during future unknown excitations. On the other hand, active control mechanisms rely on huge external energy resources which can throw them out of the loop and make them unreliable during severe seismic events. In this research, the

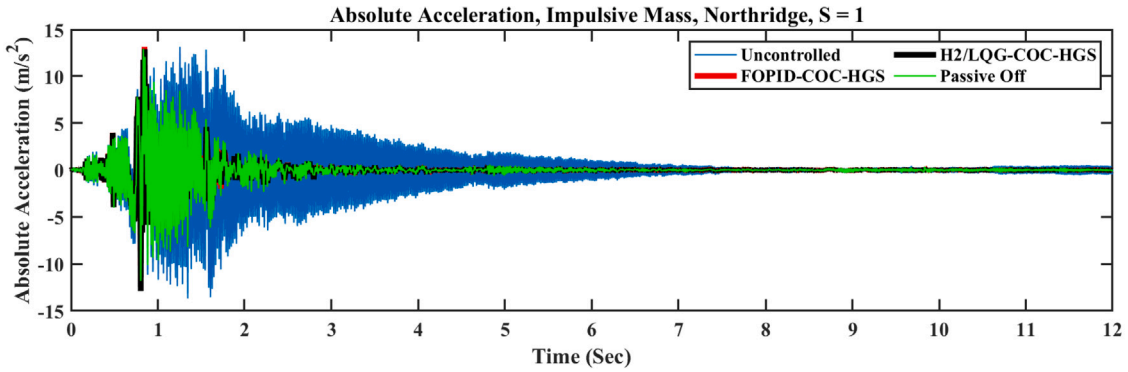

Fig. 5. Absolute acceleration time history of the impulsive mass under the Northridge earthquake, $S = 1.00$.

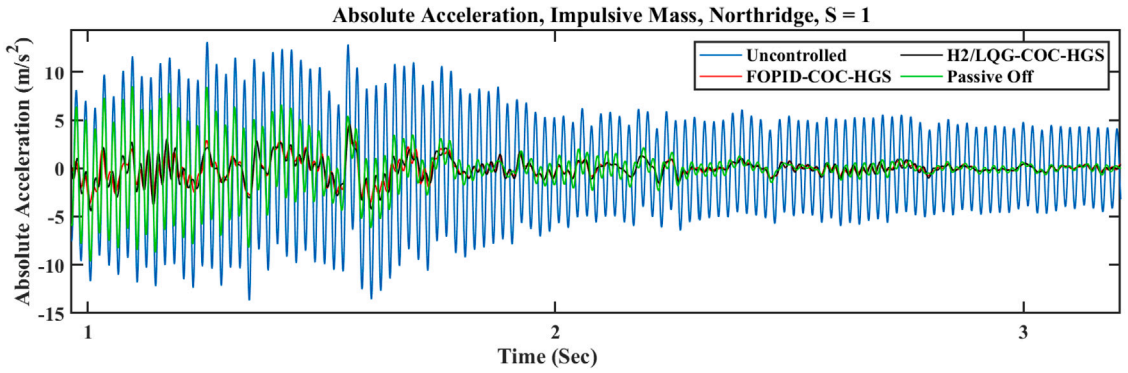

Fig. 6. Absolute acceleration time history of the impulsive mass under the Northridge earthquake, $S = 1.00$, close-up.

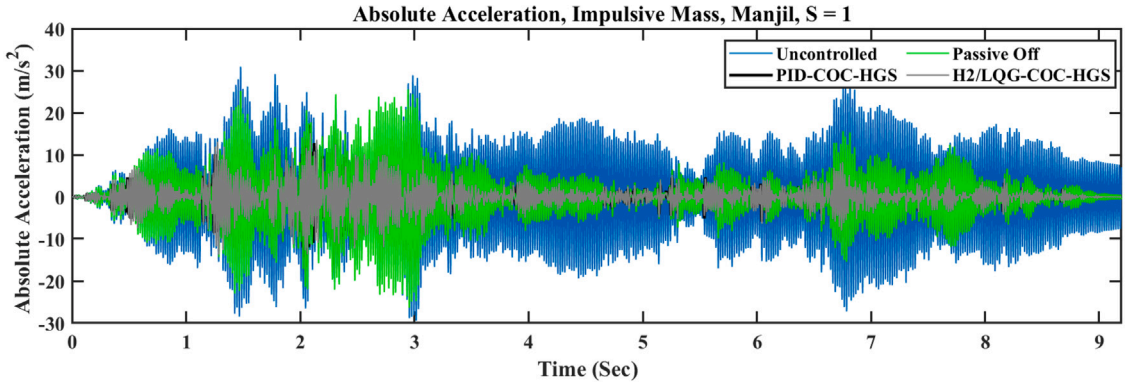

Fig. 7. Absolute acceleration time history of the impulsive mass under the Manjil earthquake, $S = 1.00$.

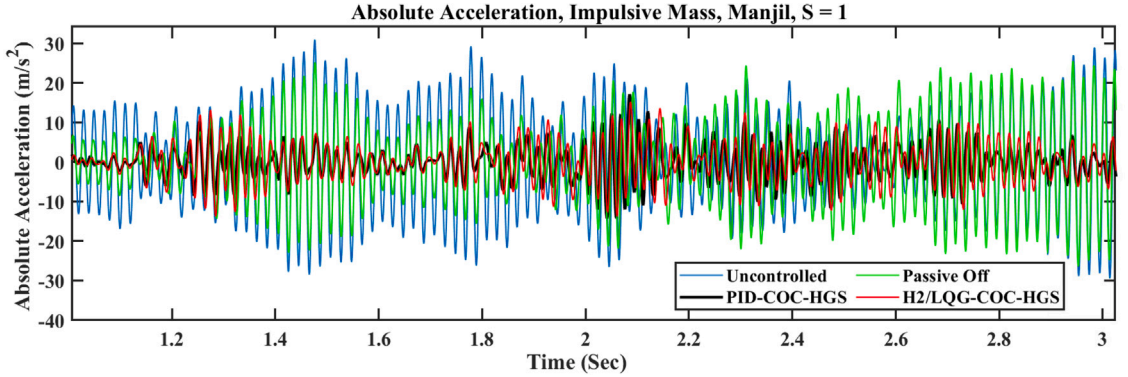

Fig. 8. Absolute acceleration time history of the impulsive mass under the Manjil earthquake, $S = 1.00$, close-up.

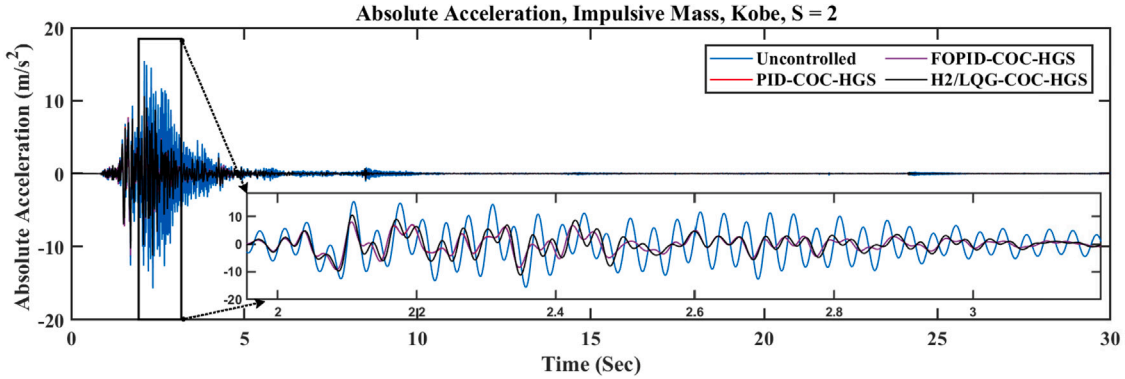

Fig. 9. Absolute acceleration time history of the impulsive mass under the Kobe earthquake, $S = 2.00$.

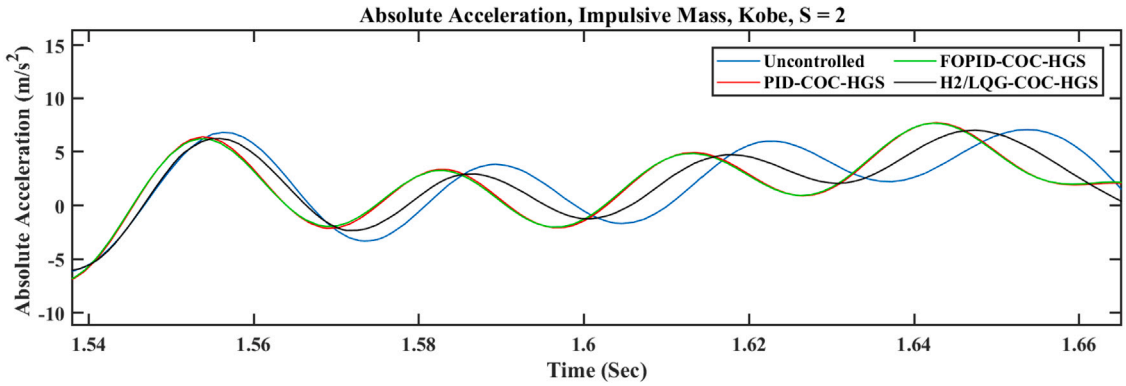

Fig. 10. Absolute acceleration time history of the impulsive mass under the Kobe earthquake, $S = 2.00$, close-up.

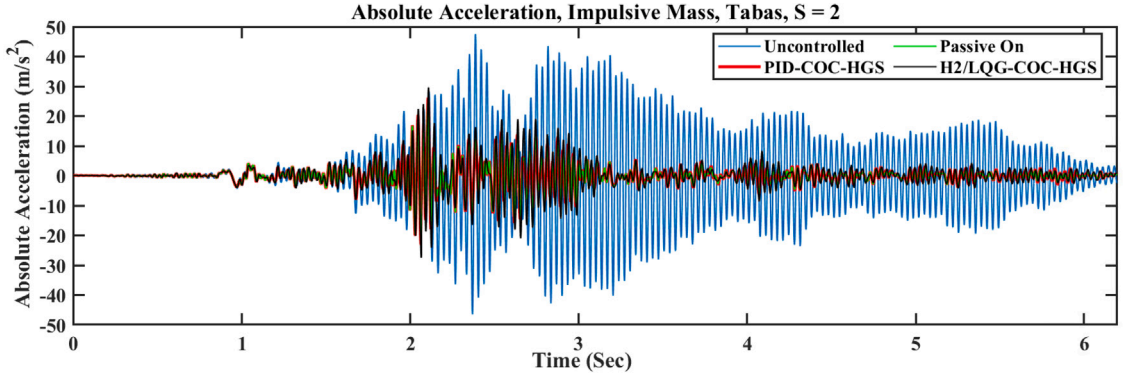

Fig. 11. Absolute acceleration time history of the impulsive mass under the Tabas earthquake, $S = 2.00$.

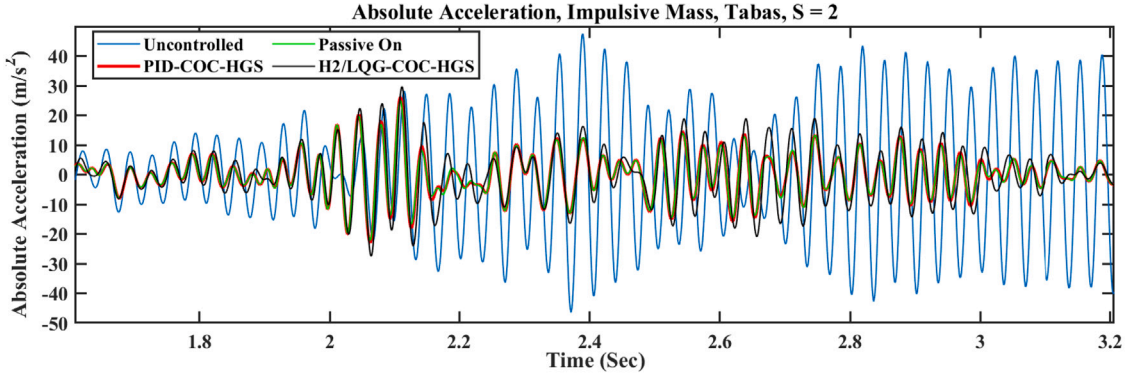

Fig. 12. Absolute acceleration time history of the impulsive mass under the Tabas earthquake, $S = 2.00$, close-up.

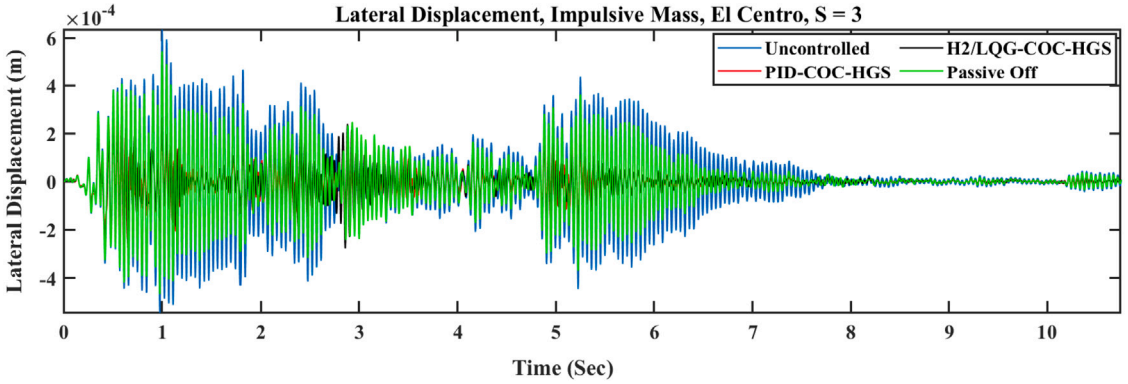

Fig. 13. Lateral displacement time history of impulsive mass under El Centro earthquake, $S = 3.00$.

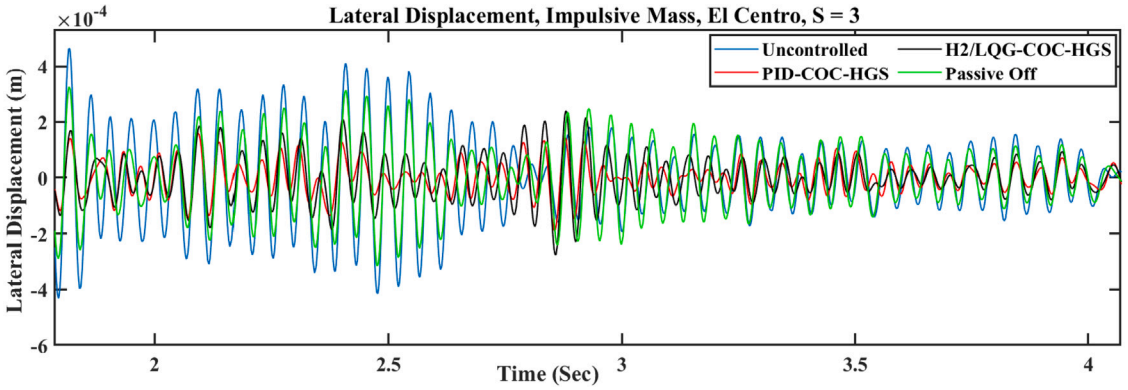

Fig. 14. Lateral displacement time history of impulsive mass under El Centro earthquake, $S = 3.00$, close-up.

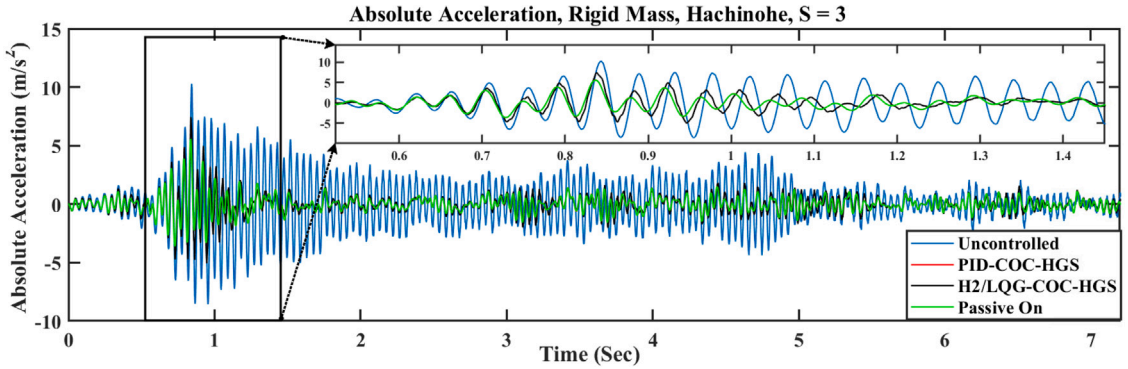

Fig. 15. Absolute acceleration time history of rigid mass under Hachinohe earthquake, $S = 3.00$.

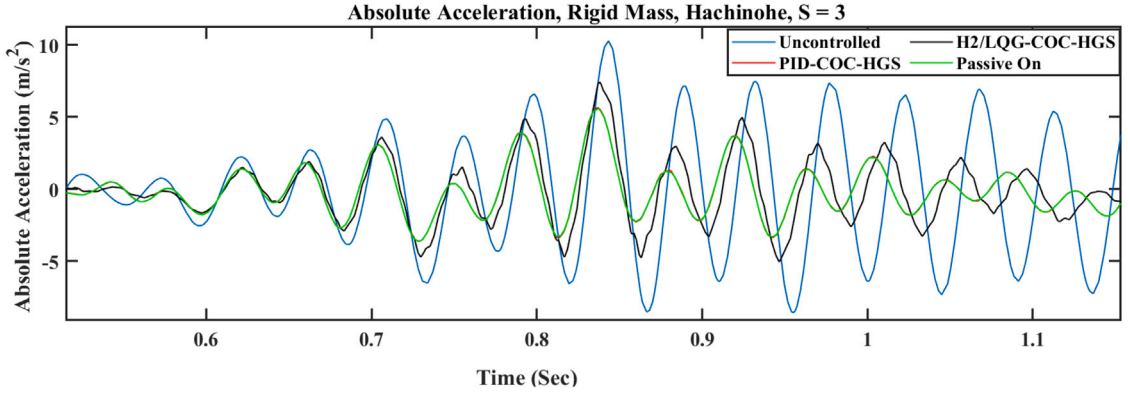

Fig. 16. Absolute acceleration time history of rigid mass under Hachinohe earthquake, $S = 3.00$, close-up.

Table 5
Performance indices for the applied control strategies to the fluid-tank-MR system.

Performance index	Control technique	El Centro	Hachinohe	Kobe	Northridge	Manjil	Tabas
			$S = 1.00$ ($Broad\ tank$)				
PI_1	PID-COC-HGS	0.2951	0.5625	0.5565	0.7680	0.4637	0.2931
	FOPID-COC-HGS	0.3033	0.5625	0.5565	0.7760	0.4568	0.2890
	H2/LQG-COC-HGS	0.3934	0.6250	0.6694	0.8800	0.4587	0.4069
	Passive On	0.2951	0.5625	0.5565	0.7520	0.4546	0.2840
	Passive Off	0.7459	0.9375	0.8387	0.8960	0.8477	0.8211
PI_2	PID-COC-HGS	0.3870	0.6755	0.6438	0.9706	0.5494	0.3580
	FOPID-COC-HGS	0.3879	0.6755	0.6463	0.9752	0.5444	0.3679
	H2/LQG-COC-HGS	0.5009	0.7383	0.6972	0.9611	0.8587	0.5927
	Passive On	0.3867	0.6770	0.6469	0.9600	0.5427	0.3520
	Passive Off	0.7505	0.8549	0.8540	0.9591	0.6151	0.7844
PI_3	PID-COC-HGS	0.3088	0.5833	0.5612	0.7914	0.4729	0.2997
	FOPID-COC-HGS	0.3088	0.5833	0.5683	0.7986	0.4663	0.2958
	H2/LQG-COC-HGS	0.3971	0.6389	0.6619	0.8849	0.4621	0.4122
	Passive On	0.3015	0.5833	0.5683	0.7770	0.4641	0.2907
	Passive Off	0.7500	0.9167	0.8345	0.8993	0.8452	0.8200
PI_4	PID-COC-HGS	0.3889	0.6633	0.6208	0.9571	0.5534	0.3584
	FOPID-COC-HGS	0.3900	0.6633	0.6234	0.9619	0.5485	0.3549
	H2/LQG-COC-HGS	0.4328	0.6950	0.6767	0.9448	0.4917	0.4587
	Passive On	0.3889	0.6646	0.6240	0.9441	0.5489	0.3501
	Passive Off	0.7549	0.8492	0.8446	0.9473	0.8523	0.8101
			$S = 2.00$ ($Slender\ tank$)				
PI_1	PID-COC-HGS	0.2789	0.4851	0.6390	0.6018	0.3170	0.4909
	FOPID-COC-HGS	0.2789	0.4851	0.6416	0.6238	0.3197	0.4845
	H2/LQG-COC-HGS	0.3553	0.6791	0.6597	0.5819	0.3826	0.5915
	Passive On	0.2789	0.4851	0.6416	0.5819	0.3140	0.5373
	Passive Off	0.8368	0.9478	0.9247	0.8164	0.7858	0.8753
PI_2	PID-COC-HGS	0.3343	0.6384	0.7522	0.7027	0.3644	0.5528
	FOPID-COC-HGS	0.3353	0.6375	0.7541	0.7228	0.3669	0.5266
	H2/LQG-COC-HGS	0.4010	0.7654	0.7387	0.6455	0.4127	0.6197
	Passive On	0.3334	0.6349	0.7566	0.6944	0.3747	0.6130
	Passive Off	0.8248	0.9556	0.9334	0.8142	0.7809	0.8782
PI_3	PID-COC-HGS	0.2883	0.5000	0.6503	0.6167	0.3271	0.4990
	FOPID-COC-HGS	0.2883	0.5000	0.6526	0.6414	0.3264	0.4932
	H2/LQG-COC-HGS	0.3581	0.6859	0.6682	0.5882	0.3878	0.5958
	Passive On	0.2860	0.5000	0.6526	0.5996	0.3248	0.5474
	Passive Off	0.8378	0.9487	0.9265	0.8178	0.7864	0.8736
PI_4	PID-COC-HGS	0.3407	0.5915	0.7134	0.7084	0.3890	0.5510
	FOPID-COC-HGS	0.3408	0.5888	0.7154	0.7253	0.3918	0.5459
	H2/LQG-COC-HGS	0.3891	0.7467	0.7163	0.6288	0.4203	0.6209
	Passive On	0.3401	0.5929	0.7167	0.6998	0.3893	0.6089
	Passive Off	0.8464	0.9567	0.9307	0.8234	0.7907	0.8775
			$S = 3.00$ ($Slender\ tank$)				
PI_1	PID-COC-HGS	0.4560	0.4545	0.5166	0.5512	0.5170	0.7113
	FOPID-COC-HGS	0.4581	0.4526	0.5166	0.5537	0.5166	0.7134
	H2/LQG-COC-HGS	0.5174	0.6304	0.5780	0.6496	0.6782	0.8167
	Passive On	0.4458	0.4506	0.5141	0.5537	0.5148	0.7042
	Passive Off	0.8650	0.9387	0.8657	0.8964	0.9733	0.9501
PI_2	PID-COC-HGS	0.5270	0.5510	0.6175	0.7225	0.6034	0.7913
	FOPID-COC-HGS	0.5286	0.5461	0.6186	0.7250	0.6007	0.7936
	H2/LQG-COC-HGS	0.5691	0.7213	0.6315	0.8003	0.7432	0.9014
	Passive On	0.5190	0.5442	0.6165	0.7265	0.6031	0.7842
	Passive Off	0.8768	0.9466	0.8667	0.9190	0.9877	0.9505
PI_3	PID-COC-HGS	0.4811	0.4750	0.5370	0.5800	0.5381	0.7296
	FOPID-COC-HGS	0.4843	0.4734	0.5380	0.5830	0.5385	0.7317
	H2/LQG-COC-HGS	0.5283	0.6419	0.5900	0.6690	0.6903	0.8253
	Passive On	0.4717	0.4704	0.5350	0.5840	0.5361	0.7220
	Passive Off	0.8648	0.9408	0.8820	0.9140	0.9735	0.9509
PI_4	PID-COC-HGS	0.5673	0.5423	0.5668	0.6331	0.6065	0.7883
	FOPID-COC-HGS	0.5682	0.5380	0.5669	0.6354	0.6098	0.7905
	H2/LQG-COC-HGS	0.5655	0.6783	0.5892	0.6829	0.7307	0.8571
	Passive On	0.5551	0.5355	0.5642	0.6393	0.6099	0.7791
	Passive Off	0.8683	0.9437	0.8717	0.9028	0.9746	0.9525

application of an MR damper as a smart semi-active mechanism that combines features of both active and passive systems while removing their drawbacks has been examined. The dynamic behaviour of the coupled fluid-tank system was modelled using the simplified mechanical model which forms the basis of analysis and design for these structures in seismic design codes around the world. Further, aspect ratio as an operational condition has been regarded in simulations for examining the effectiveness of the damper on the system. The coupled fluid-tank-MR damper system has been investigated under Far-Fault and Near-Fault ground motions with different frequency contents.

Three different control scenarios including H2/LQG, PID, and FOPID, and two passive approaches including the Passive Off and Passive On were considered to examine the structural responses of the controlled structure. For the three applied semi-active control techniques and for each aspect ratio and ground motion, the deciding parameters of each controller are optimally designed using the HGS optimisation approach which has proved promising features in the literature compared to other methods. Passive control strategies show the efficiency of the damper as a passive device as this mechanism can turn into a passive mechanism in two off (no command voltage) and on (constant voltage commanded) modes. In the semi-active control scenario, the voltage is decided based on a combined control technique.

Accelerations of the system which can easily be measured through accelerometers in practical applications were used for the feedback in the control design. For the nature of the damper, a secondary control technique, namely the Clipping algorithm has been used to decide the voltage to be commanded to the damper at each time step. Four performance indices which show the performance of each controller in attenuating the lateral displacements and absolute accelerations of the rigid and impulsive masses have been calculated and compared for each controller, aspect ratio, and ground motion. Based on the conducted numerical investigations the below conclusions can be reached,

- MR damper has shown to be a promising semi-active mechanism in reducing the structural responses of legged fluid storage tanks under the base excitations. By reducing the accelerations of the impulsive and rigid mass, these dampers can mitigate the base shear and overturning moment, and hence protect these structures against damage to the legs and elephant foot buckling.
- MR damper has reduced the lateral displacements and absolute accelerations of the impulsive and rigid mass. As the frequency and stiffness of the first convective mode are much farther away from that of the rigid and impulsive mass, this damper did not show much effect on this mode in the current configuration.
- The amount of reduction percentage points of the structural responses of the fluid tank and the performance indices of the controllers depend on the aspect ratio of the tank and the frequency content of the base excitation.
- By increasing the aspect ratio of the tank from 1 to 3, substantial changes in the frequency of the first impulsive mode are observed, however, the frequency of the first convective mode is not affected considerably. Starting from the aspect ratio 2, the reduction percentage points in the structural responses tend to become closer together under all the applied ground motions with different frequency contents. Under most of the considered ground motions and control techniques, for the aspect ratio of 3 with a first impulsive frequency much closer to the dominant frequencies in the applied ground motions, reduction percentage points become the closest together.
- Considering the four performance indices defined to evaluate the applied controllers, for all aspect ratios and under all ground motions, the PID-COC-HGS and FOPID-COC-HGS contributed the most to the seismic response attenuation of the fluid tank.

CRediT authorship contribution statement

Seyed Ehsan Aghakouchaki Hosseini: Writing – review & editing, Writing – original draft, Visualization, Methodology, Investigation, Formal analysis, Conceptualization. **Sherif Beskhyroun:** Writing – review & editing, Supervision, Resources, Project administration, Funding acquisition.

Declaration of competing interest

The authors declare that they have no known competing financial interests or personal relationships that could have appeared to influence the work reported in this paper.

Acknowledgements

Funding: This work was supported by the Earthquake Commission (EQC), Wellington, New Zealand [research grant No. 19/U780] within the Department of Built Environment Engineering, Faculty of Design and Creative Technologies, School of Future Environments, Auckland University of Technology (AUT), Auckland, New Zealand.

References

[1] Building Seismic Safety Council. NEHRP commentary on the guidelines for the seismic rehabilitation of buildings (FEMA publication 274). 1997, ATC-33 Project, Washington, DC.
[2] Dizhur D, Simkin G, Giaretton M, Loporcaro G, Palermo A, Ingham J. Performance of winery facilities during the 14 November 2016 Kaikōura earthquake. Bull New Zealand Soc Earthq Eng 2017;50(2):206–24. http://dx.doi.org/10.5459/bnzsee.50.2.206-224.
[3] Steinbrugge KV, Flores A R. The Chilean earthquakes of May, 1960: A structural engineering viewpoint. Bull Seismol Soc Am 1963;53(2):225–307.
[4] Rosewitz J, Kahanek C. Performance of wine storage tanks: Lessons from the earthquakes near Marlborough. In: Australasian structural engineering conference. ASEC, 2014.
[5] Morris GJ, Bradley BA, Walker A, Matuschka T. Ground motions and damage observations in the Marlborough region from the 2013 Lake Grassmere earthquake. Bull New Zealand Soc Earthq Eng 2013;46(4):169–87, URL https://www.bulletin.nzsee.org.nz/index.php/bnzsee/article/view/173.
[6] Yazdanian M, Ingham JM, Lomax W, Wood R, Dizhur D. Damage observations and remedial options for approximately 1500 legged and flat- based liquid storage tanks following the 2016 Kaikōura earthquake. Structures 2020;24(February):357–76. http://dx.doi.org/10.1016/j.istruc.2020.01.024.
[7] Haroun MA. Vibration studies and tests of liquid storage tanks. Earthq Eng Struct Dyn 1983;11(2):179–206.
[8] Veletsos AS. Seismic response and design of liquid storage tanks. Guidelines for the seismic design of oil and gas pipeline systems. 1984, p. 255–370.
[9] Moradi R, Behnamfar F, Hashemi S. Mechanical model for cylindrical flexible concrete tanks undergoing lateral excitation. Soil Dyn Earthq Eng 2018;106:148–62.
[10] Yazdanian M, Ingham J, Dizhur D. A conspectus of wine storage tank damage data following the 2013 and 2016 New Zealand earthquakes. 2019.
[11] Hosseini SEA, Beskhyroun S. Fluid storage tanks: A review on dynamic behaviour modelling, seismic energy-dissipating devices, structural control, and structural health monitoring techniques. In: Structures, vol. 49, Elsevier; 2023, p. 537–56.
[12] EN B. Eurocode 8: Design of structures for earthquake resistance- part 4: Silos, tanks and pipelines. Belgium: European Committee for Standardization Brussels; 2006.
[13] NZSEE. Seismic design of storage tanks. New Zealand National Society for Earthquake Engineering; 2009.
[14] Hernandez-Hernandez D, Larkin T, Chouw N. Evaluation of the adequacy of a spring-mass model in analyses of liquid sloshing in anchored storage tanks. Earthq Eng Struct Dyn 2021;50(14):3916–35.
[15] Robinson W, Tucker A. A lead-rubber shear damper. Bull New Zealand Soc Earthq Eng 1977;10(3):151–3.
[16] Chen X, Li C. Seismic performance of tall pier bridges retrofitted with lead rubber bearings and rocking foundation. Eng Struct 2020;212:110529.
[17] Kataria NP, Jangid R. Seismic protection of the horizontally curved bridge with semi-active variable stiffness damper and isolation system. Adv Struct Eng 2016;19(7):1103–17.
[18] Paolacci F, Giannini R, De Angelis M. Seismic response mitigation of chemical plant components by passive control techniques. J Loss Prev Process Ind 2013;26(5):924–35.
[19] Rawat A, Matsagar V. An oblate spheroid base isolator and floating surface diaphragm for seismic protection of liquid storage tank. J Earthq Eng 2022;26(10):5447–75.
[20] Safari S, Tarinejad R. Parametric study of stochastic seismic responses of base-isolated liquid storage tanks under near-fault and far-fault ground motions. J Vib Control 2018;24(24):5747–64. http://dx.doi.org/10.1177/1077546316647576, URL https://journals.sagepub.com/doi/abs/10.1177/1077546316647576.
[21] Tsipianitis A, Tsompanakis Y. Optimizing the seismic response of base-isolated liquid storage tanks using swarm intelligence algorithms. Comput Struct 2021;243:106407.
[22] Hasheminejad SM, Mohammadi MM, Jarrahi M. Liquid sloshing in partly-filled laterally-excited circular tanks equipped with baffles. J Fluids Struct 2014;44:97–114.
[23] Sun Y, Zhou D, Wang J, Han H. Lumped parameter model for liquid sloshing in a cylindrical tank equipped with multiple annular baffles. J Struct Eng 2021;147(5):04021042. http://dx.doi.org/10.1061/(asce)st.1943-541x.0002972.

[24] Hernández E, Santamarina D. Active control of sloshing in containers with elastic baffle plates. Int J Numer Methods Eng 2012;91(6):604–21. http://dx.doi.org/10.1002/nme.4283, URL https://onlinelibrary.wiley.com/doi/abs/10.1002/nme.4283.

[25] Mehrvarz A, Najafi Ardekani A, Khodaei MJ, Jalili N. Vibration analysis and control of fluid containers using piezoelectrically-excited side wall. J Vib Control 2019;25(7):1393–408. http://dx.doi.org/10.1177/1077546318822374.

[26] Iemura H, Igarashi A, Kalantari A. Enhancing dynamic performance of liquid storage tanks by semi-active controlled dampers. In: 13th world conference on earthquake engineering. vancouver, BC, Canada, 2004.

[27] Kobayashi N, Koyama Y. Semi-active sloshing suppression control of liquid in vessel with bulkhead. J Press Vessel Technol 2010;132(5). http://dx.doi.org/10.1115/1.4001194.

[28] Shrimali MK, Kasar AA. Seismic response of connected liquid tanks with MR dampers. In: 15th World Conference on Earthquake Engineering. 2012.

[29] Dyke SJ, Spencer Jr B, Sain M, Carlson J. Modeling and control of magnetorheological dampers for seismic response reduction. Smart Mater Struct 1996;5(5):565.

[30] Zhang Z, Peng Y. Dynamic physical model for MR damper considering chain deflection in preyield stage. J Eng Mech 2020;146(11):04020122.

[31] Ahamed R, Choi S-B, Ferdaus MM. A state of art on magneto-rheological materials and their potential applications. J Intell Mater Syst Struct 2018;29(10):2051–95.

[32] Madhekar SN, Jangid RS. Variable dampers for earthquake protection of benchmark highway bridges. Smart Mater Struct 2009;18(11):115011. http://dx.doi.org/10.1088/0964-1726/18/11/115011.

[33] Chen P-C, Tsai K-C, Lin P-Y. Real-time hybrid testing of a smart base isolation system. Earthq Eng Struct Dyn 2014;43(1):139–58.

[34] Prakash S, Jangid R. Seismic response of isolated structures with an improved model of the UFREI. In: Structures, vol. 42, Elsevier; 2022, p. 434–48.

[35] Colombo J, Almazán J. Experimental investigation on the seismic isolation for a legged wine storage tank. J Constr Steel Res 2017;133:167–80.

[36] Ogunmakinde OE, Egbelakin T, Omotayo T, Sojobi A. Seismic vulnerability and inventory of at-risk elements in the wine industry: Auckland region case study. In: Structures, vol. 58, Elsevier; 2023, 105346.

[37] Colombo J, Wilches J, Leon R. Seismic fragility of legged liquid storage tanks based on soil type classifications. J Constr Steel Res 2022;192:107212.

[38] Hosseini SEA, Beskhyroun S. Seismic vibration control of fluid storage tanks using magnetorheological dampers. In: ACMSM26: Proceedings of the 26th Australasian conference on the mechanics of structures and materials. Springer Singapore; 2024.

[39] Haroun MA, Housner GW. Seismic design of liquid storage tanks. J Tech Counc ASCE 1981;107(1):191–207.

[40] Shrimali M, Jangid R. Seismic analysis of base-isolated liquid storage tanks. J Sound Vib 2004;275(1–2):59–75.

[41] Zhu H, Tang Z, Luo H. Seismic performance of a base-isolated flexible liquid storage tank equipped with a novel rate-independent damping device. In: Structures, vol. 51, Elsevier; 2023, p. 215–25.

[42] Spencerm Jr. B, Dyke S, Sain M, Carlson J. Phenomenological model for magnetorheological dampers. J Eng Mech 1997;123(3):230–8.

[43] Dominguez A, Sedaghati R, Stiharu I. Modeling and application of MR dampers in semi-adaptive structures. Comput Struct 2008;86(3–5):407–15.

[44] Mohebbi M, Dadkhah H, Rasouli Dabbagh H. Modified H2/LQG control algorithm for designing a multi-objective semi-active base isolation system. J Vib Control 2018;24(23):5693–704.

[45] Lavassani SHH, Shangapour S, Homami P, Gharehbaghi V, Farsangi EN, Yang T. An innovative methodology for hybrid vibration control (MR+ TMD) of buildings under seismic excitations. Soil Dyn Earthq Eng 2022;155:107175.

[46] Fallah AY, Taghikhany T. Time-delayed decentralized H2/LQG controller for cable-stayed bridge under seismic loading. Struct Control Health Monit 2013;20(3):354–72.

[47] Zafarani MM, Halabian AM. Supervisory adaptive nonlinear control for seismic alleviation of inelastic asymmetric buildings equipped with MR dampers. Eng Struct 2018;176:849–58.

[48] Zafarani MM, Halabian AM. A new supervisory adaptive strategy for the control of hysteretic multi-story irregular buildings equipped with MR-dampers. Eng Struct 2020;217:110786.

[49] Wani ZR, Tantray M. Study on integrated response-based adaptive strategies for control and placement optimization of multiple magneto-rheological dampers-controlled structure under seismic excitations. J Vib Control 2022;28(13–14):1712–26.

[50] Meng F, Liu S, Liu K. Design of an optimal fractional order PID for constant tension control system. IEEE Access 2020;8:58933–9.

[51] Şahin Ö, Adar NG, Kemerli M, Caglar N, Şahin İ, Parlak Z, Kükrek S, Engin T. A comparative evaluation of semi-active control algorithms for real-time seismic protection of buildings via magnetorheological fluid dampers. J Build Eng 2021;42:102795.

[52] Maiti D, Acharya A, Chakraborty M, Konar A, Janarthanan R. Tuning PID and PI/λ D δ controllers using the integral time absolute error criterion. In: 2008 4th international conference on information and automation for sustainability. IEEE; 2008, p. 457–62.

[53] Tepljakov A, Vunder V, Petlenkov E, Nakshatharan SS, Punning A, Kaparin V, Belikov J, Aabloo A. Fractional-order modeling and control of ionic polymer-metal composite actuator. Smart Mater Struct 2019;28(8):084008.

[54] Yang Y, Chen H, Heidari AA, Gandomi AH. Hunger games search: Visions, conception, implementation, deep analysis, perspectives, and towards performance shifts. Expert Syst Appl 2021;177:114864.

[55] Kamalzare M, Johnson EA, Wojtkiewicz SF. Computationally efficient design of optimal strategies for controllable damping devices. Struct Control Health Monit 2015;22(1):1–18.

[56] Abdeddaim M, Djerouni S, Ounis A, Athamnia B, Farsangi EN. Optimal design of magnetorheological damper for seismic response reduction of base-isolated structures considering soil-structure interaction. In: Structures, vol. 38, Elsevier; 2022, p. 733–52.

[57] Podlubny I. Fractional-order systems and PI/sup/spl lambdad/sup/spl mu-controllers. IEEE Trans Autom Control 1999;44(1):208–14.

[58] Wang Y, Dyke SJ. A comparative study of the base isolation benchmark problem using h2/lqg and smart dampers. In: Structures congress 2006: 17th analysis and computation specialty conference. 2006, p. 1–16.

[59] Sorenson HW. Kalman filtering techniques. In: Advances in control systems, vol. 3, Elsevier; 1966, p. 219–92.

[60] Baltieri M, Buckley CL. On kalman-bucy filters, linear quadratic control and active inference. 2020, arXiv preprint arXiv:2005.06269.

[61] Ji M, Lyu Y, Pan Q, Wei G, Wei D. Adaptive control of uncertain systems with input delay based on active inference. In: International conference on autonomous unmanned systems. Springer; 2022, p. 2810–22.

[62] Sreenivasappa B, Udaykumar R. Analysis and implementation of discrete time PID controllers using FPGA. Int J Electric Comput Eng 2010;2(1):71–82.

[63] Zand JP, Sabouri J, Katebi J, Nouri M. A new time-domain robust anti-windup PID control scheme for vibration suppression of building structure. Eng Struct 2021;244:112819.

[64] Dubey V, Goud H, Sharma PC. Role of PID control techniques in process control system: a review. In: Data engineering for smart systems: Proceedings of SSIC 2021. Springer; 2022, p. 659–70.

[65] Zhang H, Trott G, Paul R. Minimum delay PID control of interpolated joint trajectories of robot manipulators. IEEE Trans Ind Electron 1990;37(5):358–64.

[66] Shaban E, Sayed H, Abdelhamid A. A novel discrete PID+ controller applied to higher order/time delayed nonlinear systems with practical implementation. Int J Dyn Control 2019;7:888–900.

[67] Slate J, Sheppard L. Automatic control of blood pressure by drug infusion. IEE Proc A 1982;129(9):639–45.

[68] Marchetti G, Barolo M, Jovanovic L, Zisser H, Seborg DE. An improved PID switching control strategy for type 1 diabetes. IEEE Trans Biomed Eng 2008;55(3):857–65.

[69] Glickman S, Kulessky R, Nudelman G. Identification-based PID control tuning for power station processes. IEEE Trans Control Syst Technol 2004;12(1):123–32.

[70] Oustaloup A, Sabatier J, Moreau X. From fractal robustness to the CRONE approach. In: Proc., ESAIM, Vol. 5. 1998, p. 177–92.

[71] Kumar VB, Sampath D, Praneeth VS, Kumar YP. Error performance index based PID tuning methods for temperature control of heat exchanger system. In: 2021 IEEE international IOT, electronics and mechatronics conference. IEEE; 2021, p. 1–6.

[72] Daful AG. Comparative study of PID tuning methods for processes with large & small delay times. In: 2018 advances in science and engineering technology international conferences. IEEE; 2018, p. 1–7.

[73] Rao CS, Santosh S, et al. Tuning optimal PID controllers for open loop unstable first order plus time delay systems by minimizing ITAE criterion. IFAC-PapersOnLine 2020;53(1):123–8.

[74] Joseph SB, Dada EG, Abidemi A, Oyewola DO, Khammas BM. Metaheuristic algorithms for PID controller parameters tuning: Review, approaches and open problems. Heliyon 2022;8(5).

[75] Falcone R, Lima C, Martinelli E. Soft computing techniques in structural and earthquake engineering: a literature review. Eng Struct 2020;207:110269.

[76] Harirchian E, Hosseini SEA, Jadhav K, Kumari V, Rasulzade S, Işık E, et al. A review on application of soft computing techniques for the rapid visual safety evaluation and damage classification of existing buildings. J Build Eng 2021;43:102536.

[77] Flah M, Nunez I, Ben Chaabene W, Nehdi ML. Machine learning algorithms in civil structural health monitoring: a systematic review. Arch Comput Methods Eng 2021;28(4):2621–43.

[78] Katoch S, Chauhan SS, Kumar V. A review on genetic algorithm: past, present, and future. Multimedia Tools Appl 2021;80:8091–126.

[79] Shami TM, El-Saleh AA, Alswaitti M, Al-Tashi Q, Summakieh MA, Mirjalili S. Particle swarm optimization: A comprehensive survey. IEEE Access 2022;10:10031–61.

[80] Nayar N, Gautam S, Singh P, Mehta G. Ant colony optimization: A review of literature and application in feature selection. In: Inventive computation and information technologies: Proceedings of ICICIT 2020. Springer; 2021, p. 285–97.

[81] Heidari AA, Mirjalili S, Faris H, Aljarah I, Mafarja M, Chen H. Harris hawks optimization: Algorithm and applications. Future Gener Comput Syst 2019;97:849–72.

[82] Mirjalili S, Mirjalili SM, Lewis A. Grey wolf optimizer. Adv Eng Softw 2014;69:46–61.